JNC TY9400 2005-020

Study on Pb-Bi Corrosion of Structural and Fuel Cladding Materials for Nuclear Applications

Part VI. Results of Exposure Experiments in Oxygen Containing Flowing LBE at 550 °C for 10,000h

August 2005

Japan Nuclear Cycle Development Institute
Forschungszentrum Karlsruhe GmbH

〒319-1184　茨城県那珂郡東海村村松４番地49

核燃料サイクル開発機構

技術展開部　技術協力課

電話：029-282-1122

ファックス：029-282-7980

電子メール：jserv@jnc.go.jp

Study on Pb-Bi Corrosion of Structural and Fuel Cladding Materials for Nuclear Applications

Part VI. Results of Exposure Experiments in Oxygen Containing Flowing LBE at 550 °C for 10,000h

C. Schroer[*], Z. Voß[*], O. Wedemeyer[*], J. Novotny[*],
J. Konys[*], A. Heinzel[**], A. Weisenburger[**], G. Müller[**],
T. Furukawa[***], K. Aoto[***]

Abstract

This report summarises the results of exposure experiments on the behaviour of 12Cr-2W steel P122 and an 9Cr-2W ODS-steel in oxygen-containing flowing lead-bismuth eutectic (LBE) at 550°C, which were performed in the CORRIDA loop at the Karlsruhe Lead Laboratory (KALLA) as part of the collaboration between the Japan Nuclear Cycle Development Institute and the Karlsruhe Research Centre. The duration of these experiments was nominally 800, 2000, 5000 and 10,000 h.

Both steels were tested after surface-finishing by turning and after surface alloying with aluminium in the GESA-facility. Owing to initial problems with the enrichment of oxygen in the flowing LBE, the oxygen content considerably varied during most of these experiments, so that the influence of temporary changes in the oxygen content of the LBE could also be investigated.

The behaviour of P122 and ODS at permanently high oxygen content was deduced from an experiment for 4990 h at 550°C and ($c_O \approx 5\times10^{-7}$ mass-% or $a_{PbO} \approx 10^{-3}$). The results are compared with the findings of exposures to stagnant LBE at 550°C and $c_O = 10^{-6}$ mass-% (COSTA-experiments).

[*] Institute for Materials Research III, Forschungszentrum Karlsruhe GmbH (FZK)

[**] Institute for Pulsed Power and Microwave Technology, FZK

[***] Advanced Material Research Group, Advanced Technology Division, O-arai Engineering Center, Japan Nuclear Cycle Development Institute

原子炉構造材料及び燃料材料の鉛ビスマス中腐食に関する研究
第 6 報 550°C 酸素濃度制御流動鉛ビスマス中 10,000 時間浸漬試験結果

C. Schroer[*], Z. Voß[*], O. Wedemeyer[*], J. Novotny[*],
J. Konys[*], A. Heinzel[**], A. Weisenburger[**], G. Müller[**],
古川智弘[***], 青砥紀身[***]

要　旨

本報告書は、P122（12Cr-2W）鋼および ODS（9Cr-2W）鋼の 550°C 酸素濃度制御流動鉛ビスマス（LBE）中腐食試験結果についてまとめたものである。この試験研究は、核燃料サイクル開発機構と独国カールスルーエ研究所との研究協力契約の下で、カールスルーエ鉛実験施設（KALLA）の CORRIDA 試験ループを用いて実施した。腐食試験時間は、800h、2,000h、5,000h および 10,000h である。

両鋼は、旋盤による試験片に加工し、その一部は KALLA 内の GESA 施設においてアルミニウム表面改質処理を施した。流動 LBE 中酸素濃度制御の初期不具合により、これら実験の大部分の期間について酸素濃度の変動を生じた。このため、LBE 中の酸素濃度が一時的に変動した場合の影響についても評価を実施した。

高い酸素濃度で推移した時の P122 および ODS 鋼の腐食挙動は、550°C-4,990h の実験結果から評価した。このときの酸素濃度と PbO の活量は、それぞれ 5×10^{-7}mass%、10^{-3} と見積もられた。このときの両鋼の腐食挙動については、停留 LBE 中腐食試験装置（COSTA）にて実施した 550°C、酸素濃度 10^{-6}mass%の試験結果と比較した。

[*] 独国・カールスルーエ研究所、Institute for Materials Research III

[**] 独国・カールスルーエ研究所、Institute for Pulsed Power and Microwave Technology

[***] 核燃料サイクル開発機構　大洗工学センター　要素技術開発部　新材料研究グループ

Table of Contents

1 Introduction

The objective of this part of the "Study on Pb/Bi Corrosion of Structural and Fuel Cladding Materials for Nuclear Applications" was to investigate the behaviour of 12Cr-2W steel P122 and a 9Cr-2W ODS-steel (referred to as ODS in the following) in oxygen-containing, flowing lead-bismuth eutectic (LBE) at 550°C. Furthermore, the effect of surface-alloying with aluminium (GESA-treatment) was examined. The respective exposure experiments for up to 10,000 h were performed in the CORRIDA loop at the Karlsruhe Lead Laboratory as part of the collaboration between the Japan Nuclear Cycle Development Institute (JNC) and the Karlsruhe Research Centre.

2 Experimental

2.1 Sample materials

The composition of the P122 sample (slice of a massive steel block) used in this investigation is shown in Table 1. Prior to slicing, the steel block (thickness ~200 mm) was autenitised at 1070°C, air-cooled and subsequently tempered at 770°C by the supplier. In general, the microstructure of P122 with nominal 12 mass-% Cr will partly consist of ferrite, since, according to the Fe-Cr phase diagram [1], autenitising is possible only in the γ-α two-phase region. The composition of the specific sample is <11 mass-%, so that the microstructure can be fully martensitic after autenitising and air-cooling. The microstructure of the P122 sample observed after autenitising and tempering is typical for tempered martensite, consisting of martensite laths within the prior austenite grains. Further constituents of tempered martensite are carbide precipitates of type $M_{23}C_6$ (especially containing Cr) which form preferentially at the prior austenite grain boundaries and at the martensite lath boundaries. Precipitated carbonitrides, M(C,N), especially containing Nb may be present within the martensite laths. For martensitic steels with 9 mass-% Cr, it was demonstrated by Ennis et al. [2,3] that dislocations initially present with high density after martensite formation transform into dislocation networks during tempering, which can significantly influence the corrosion behaviour (e.g., paths for fast Cr-diffusion), probably also in the case of martensitic steels with higher Cr content.

Table 1 – *Chemical composition (in mass-%) and final heat treatment of the P122 sample.*

P122 (HCM12A, SUS410J3)

Fe	Cr	W	Cu	Mn	Mo	Ni	Si	V	Nb	Al
bal. (84.69)	10.54	1.72	1.00	0.64	0.34	0.33	0.27	0.19	0.048	0.001

C	N	B	P	S
0.11	0.071	0.034	0.016	0.002

heat treatment (block with a thickness of ~200 mm):
100 min at 1070°C (air cooling) + 440 min at 770°C

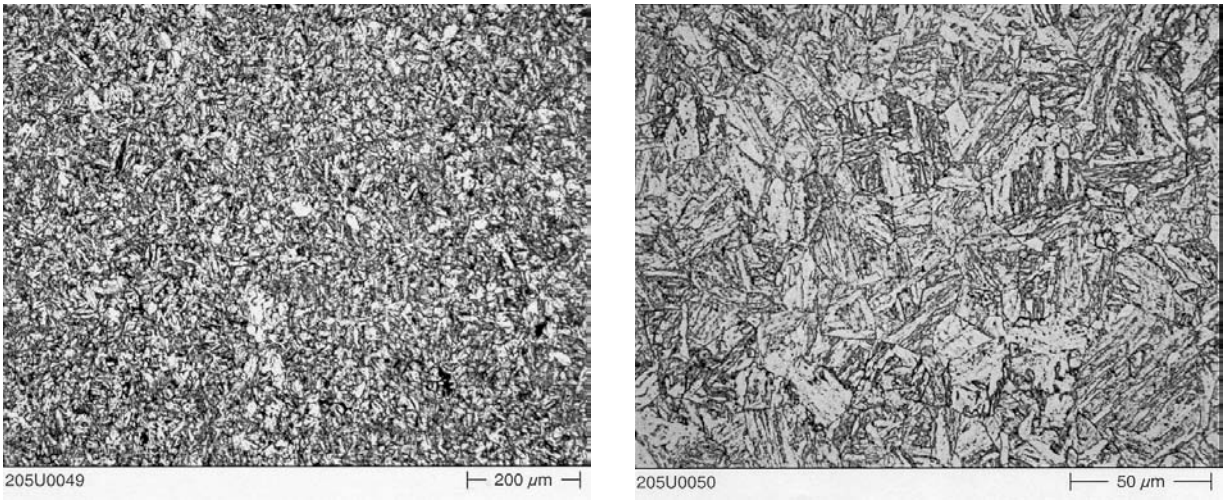

Figure 1 – *Light-optical micrographs of the microstructure of P122 in the as-received state. Etching: nitric acid.*

Table 2 – *Chemical composition (in mass-%) and final heat treatment of the ODS sample.*

ODS										
Fe	Cr	W	Y	Ti	O	C	N	Ar	S	P
bal. (88.43)	8.85	1.94	0.27	0.20	0.17	0.13	0.011	0.005	0.003	0.001
heat treatment (bar with a diameter of 10 mm): 60 min@1050°C (air cooling) + 60 min@800°C (air cooling)										

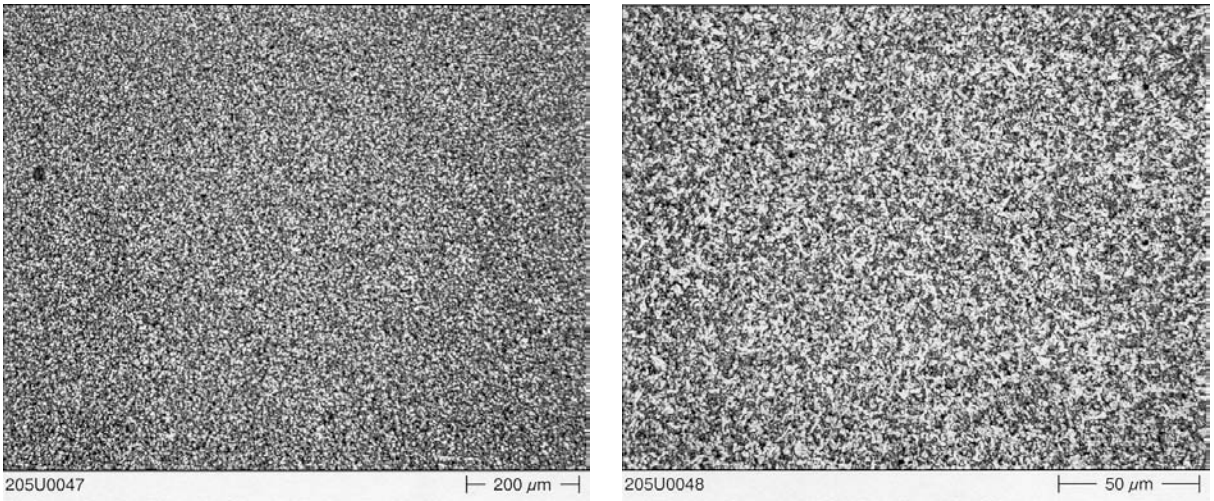

Figure 2 – *Light-optical micrographs of the microstructure of ODS in the as-received state. Etching: nitric acid.*

The chemical composition of the investigated ODS sample (bar with a diameter of 10 mm) and the final heat treatment are summarised in Table 2. The microstructure in the as-received state (after final heat treatment) is shown in Figure 2. In comparison to the P122 sample, the martensite laths (fully martensitic structure) are smaller in size and larger in number, so that the microstructure of ODS provides much more paths for fast (Cr) diffusion, in addition to the dislocation networks already mentioned in connection with the microstructure of P122. Fast Cr diffusion may be beneficial for corrosion (oxidation) resistance and partly compensates for the lower Cr content of the ODS steel in comparison to P122. The Y- and Ti-oxides dispersed in the microstructure of ODS may influence (promote) the nucleation of oxides on the steel surface.

2.2 Specimen preparation

Specimens measuring Ø8×35 mm were machined from the as-received steel samples according to the workshop drawing shown in Figure 3. The ends of the specimens were provided with an external and internal thread, respectively, so as to combine specimens of the diverse steels which are exposed in the loop at the same time to a rod of normally 16 specimens (which is then introduced into one of the test-sections of the CORRIDA loop). Unless otherwise noted, the specimen surface was finished by turning and degreased in acetone before the experiment.

The surface-alloying with aluminium was performed in the GESA facility at the Institute for Pulsed Power and Microwave Technology in the Karlsruhe Research Centre [4,5]. One quarter of the circumference of the cylindrical steel specimens was covered with a thin Al foil which was melted on the steel surface via a pulsed electron beam (Figure 4), resulting in a thin, aluminised zone at the steel surface. In a second step, the aluminised zone was homogenised by re-melting for two times in the GESA facility. Although only the upper quarter of the horizontally positioned specimens was covered with the Al foil, the surface of approximately one half of the specimen circumference is alloyed with Al. However, the desired high quality of the aluminised zone can only be expected for the central part, where the foil covered the surface. There is no persisting effect of the GESA-treatment on the reverse side (non-aluminised part of the circumference) of the cylindrical specimens, since the heat necessary for melting is introduced very locally and rather quickly dissipated by the main part of the specimens which remains solid.

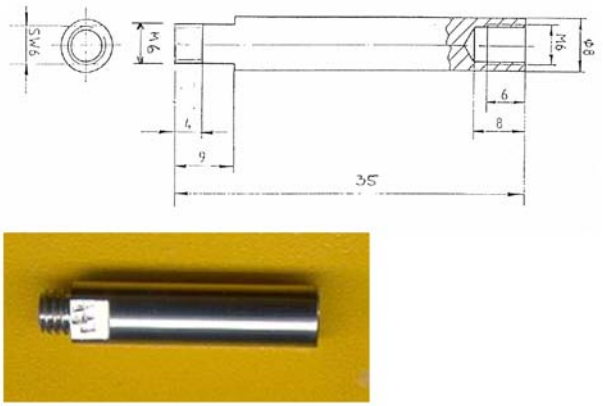

Figure 3 – *Workshop drawing according to which the specimens for the corrosion tests were machined and photograph of specimen.*

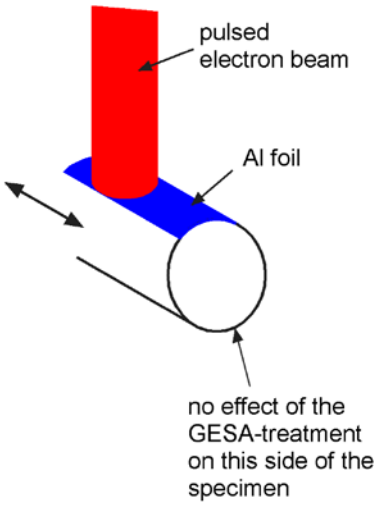

Figure 4 – *Schematic illustration of the surface-alloying with aluminium in the GESA-facility. There is no persisting effect of the GESA-treatment on the reverse side (non-aluminised part of the circumference) of the specimens.*

The Al enrichment achieved by the GESA treatment of circular specimens is exemplified in Figure 5. In order to save the effort of preparing GESA-treated specimens of P122 and ODS solely for checking the Al content at the surface, electron-probe micro-analyses (EPMA) of the aluminised zone were performed using respective specimens which had been exposed in the CORRIDA loop for 2018 h and prepared for the analysis of corrosion products; these EPMA measurements were performed at sites where, if any, only negligible corrosion of the aluminised zone occurred. According to the results, the aluminised zone at the surface of P122 contains approximately 12 mass-% Al (and 9 mass-% Cr) and extends 9 µm into the steel; after an overall distance of 17 µm from the surface, the steel exhibits the original composition (Figure 5, left). In the case of GESA-treated ODS (Figure 5, right), an Al content of approximately 6 mass-% (8 mass-% Cr) was measured for the first 5 µm and the origin-

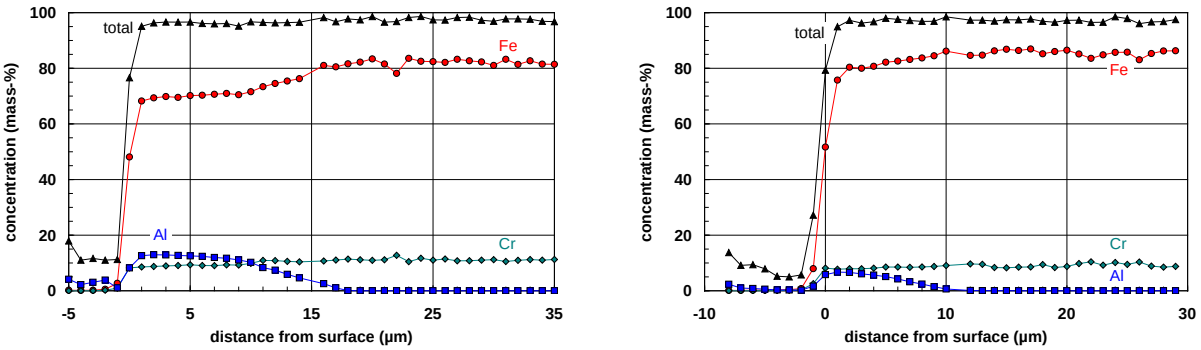

Figure 5 – *Results of electron-probe micro-analyses (EPMA) along the aluminised zone at the surface of P122 (left) and ODS (right). "Total" denotes the sum of mass concentrations determined for all of the considered elements and its deviation from 100 can be regarded as a measure of quality of the analysis. Al was calibrated using an Al_2O_3 standard which may cause a slightly higher error for Al than for the other elements in a metallic phase.*

nal composition of the steel is exhibited at >10 µm from the surface. Qualitative energy-dispersive X-ray analyses (EDX) performed on cross-sections of the aluminised surface layers (after exposure for 5016 h in the CORRIDA loop) basically affirmed the EPMA analyses with respect to the thickness of the aluminised zone, but, in the case of P122, the overall thickness was locally 25 µm. A convenient interpretation of these measurements is that the GESA treatment as applied to the cylindrical specimens of P122 and ODS produces an aluminised zone of 5-9 µm thickness with Al contents in the order of 6-12 mass-%, which smoothly merges into the original steel after another 5-8 µm. Deviations from these ranges can occur.

2.3 The CORRIDA loop

CORRIDA is a forced convection loop with a developed length of 36 m. All components are made of a 17-12 Cr-Ni steel (DIN W.-Nr. 1.4571; ~SUS316Ti). The hold-up volume of liquid Pb-Bi is approximately 1000 kg and, in the steady state, circulates at a mass-flow rate of 5.3 kg/s, resulting in a time necessary for one circulation of 190 s. A schematic illustration of the CORRIDA loop is shown in Figure 6.

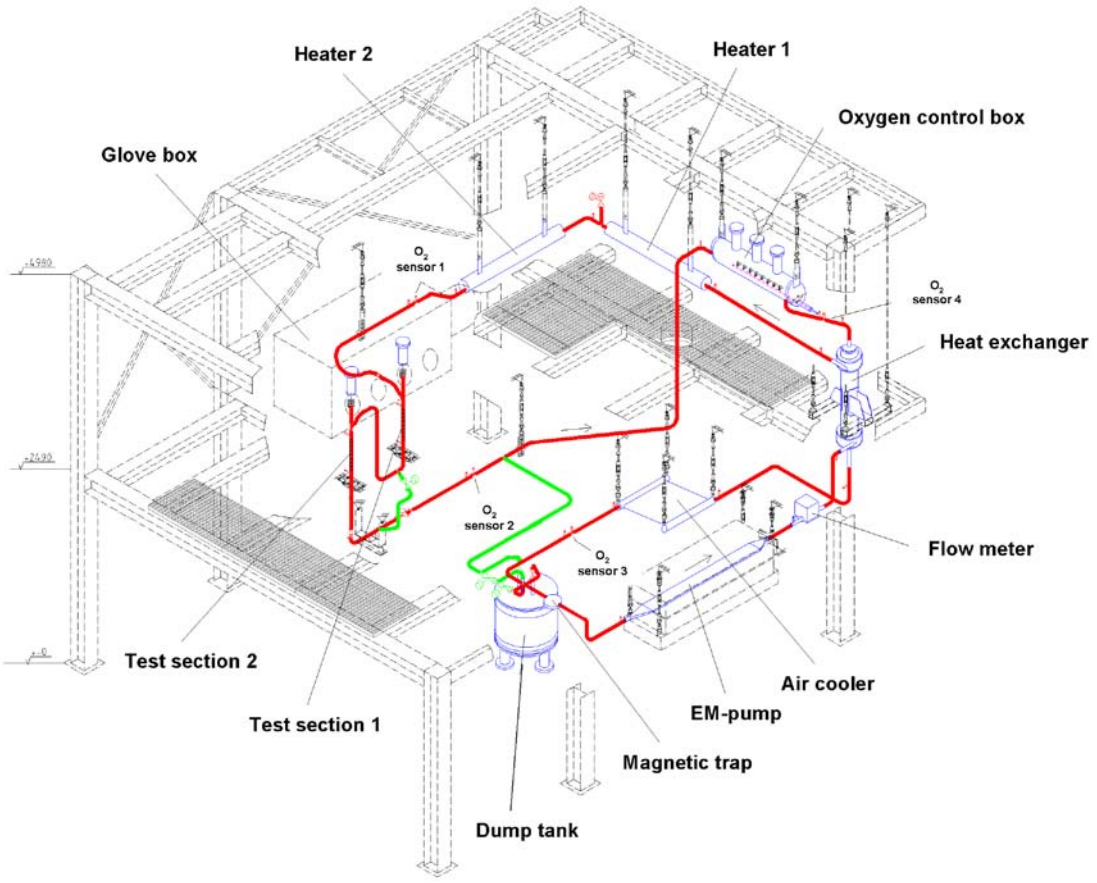

Figure 6 – *Schematic illustration of the CORRIDA loop (blue: components; red: flow path; green: additional tubing for emptying the loop). The oxygen activity in the circulating liquid metal is adjusted in the so-called "oxygen control box" via mass transfer between the liquid metal and an argon stream with variable oxygen partial pressure. The oxygen activity achieved in the melt is recorded via oxygen sensors residing in selected positions along the loop.*

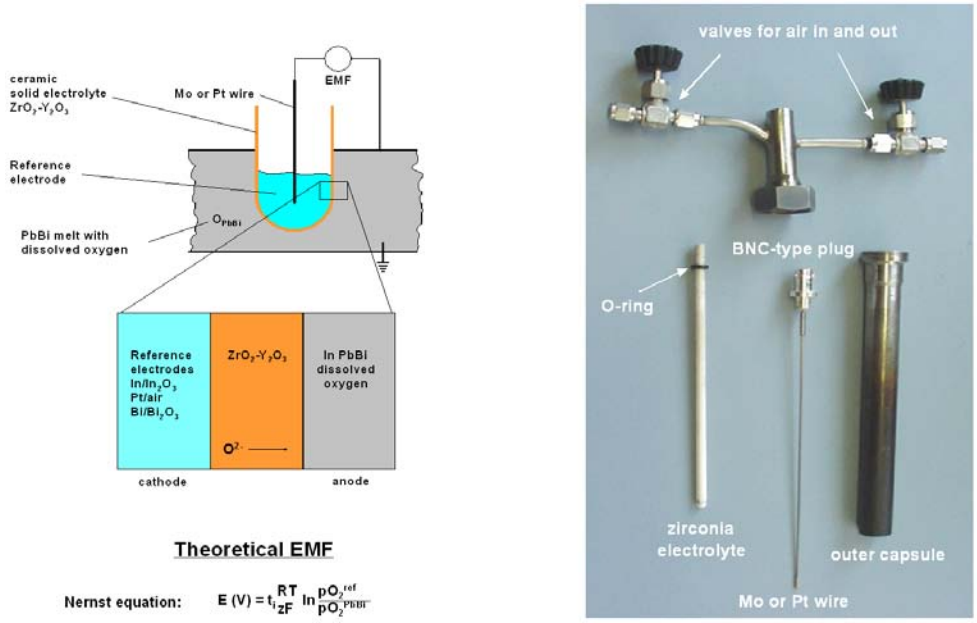

Figure 7 – *Schematic illustration of the measuring principle and photograph of the components of the used oxygen sensors.*

The circulation of the liquid metal is forced with an air-cooled electromagnetic pump which represents both the coldest (380°C) and the lowest point along the loop (except for the dump tank). A counter-flow heat-exchanger and additional heaters following in the direction of the flow increase the temperature to 550°C, the designated temperature in the two test-sections of the loop. The test-sections consist of vertical tubes with an inner diameter of 20 mm, i.e., the velocity with which the Pb-Bi passes the specimens (Ø8 mm) is 2 m/s.

The concentration (chemical potential) of oxygen dissolved in the liquid metal is controlled in a tank (oxygen-control box; OCB) which is located past the test-sections in the direction of flow for hydrostatic reasons and is kept at 550°C. The Pb-Bi flows through the OCB simultaneously with an oxygen-containing gas stream which is fed in above the liquid-metal surface (optionally via a lance immersed at the bottom of the OCB). The Pb-Bi absorbs oxygen when the chemical potential of oxygen in the liquid metal is lower than in the gas; in the case of reverse conditions, oxygen is released from the liquid. The instantaneous chemical potential (activity) of oxygen in the Pb-Bi is measured in selected positions along the loop (up- and downstream of the test-sections, downstream of the oxygen-control system and in the cold part of the loop) using zirconia solid-electrolyte sensors with platinum (Pt)/air or Bi/bismuth oxide (Bi_2O_3) as oxygen-reference systems (Figure 7) [6,7]. After leaving the OCB, the Pb-Bi is cooled in the cold side of the counter-flow heat-exchanger and an additional air-cooler, before entering the pump again.

When the designated exposure time of specimens is reached, the pumping power is reduced so that the locks above the test-sections can be opened during operation. The specimen rods are removed from the test-sections, the respective specimens are substituted by new ones and the rods are then re-introduced into the loop. The specimen exchange is performed in a glove-box flushed with Ar, so as to prevent

significant contamination of the Pb-Bi with oxygen. Slight oxidation of hot Pb-Bi adhering to the specimens (especially formation of PbO) is possible.

Some more details of the CORRIDA loop can be found in Reference 8.

2.4 Testing conditions

The Pb-Bi alloy employed in the CORRIDA loop consists of 46 mass-% Pb, which practically coincides with the composition of the lead-bismuth eutectic (LBE: 44.8 mass-% Pb; Tmp=125.5°C). The Pb and Bi thermodynamic activities at 550°C are a_{Pb}=0.370 and a_{Bi}=0.462, in comparison to 0.357 and 0.477 for LBE [9]. For calculations which require thermodynamic activities of the liquid metal components, the actual composition of the alloy was used.

2.4.1 Measurement of the oxygen content

Since the oxygen content of the LBE is an important parameter of the corrosion test, the calculation of the oxygen mass concentration, c_O, from the signal of the oxygen sensors is briefly discussed.

The electromotive force (EMF or E in mathematical equations) indicated by the zirconia solid-electrolyte oxygen sensors employed along the loop is related to the oxygen activity a_{O_2} in the LBE (reference state: pure gaseous oxygen, O_2, at 1 bar (10^5Pa) and the temperature under consideration) according to the Nernst equation, i.e.,

$$a_{O_2} = p_{O_2;ref}/(\text{bar}) \exp\left\{-46{,}418 \frac{E/(V)}{T/(K)}\right\} \quad (1)$$

$p_{O_2;ref}$ is the oxygen partial pressure inside the solid-electrolyte sensor, which is determined by the reference system (metal/gas or metal/metal oxide) used. The knowledge of a_{O_2} is sufficient for characterising the testing conditions with respect to the thermodynamic stability of oxides and driving-forces, e.g., for oxygen transport through oxide scales. In the case of the CORRIDA loop, the oxygen activity in the LBE which is relevant for the test-sections is measured by an Pt/air sensor ($p_{O_2;ref}$ = 0.20946 bar (0.20946 X 10^5 Pa) for dry air) which resides near the inlet of the first test-section at 553°C.

When convective transport along the non-isothermal loop has to be considered (since oxygen sensors cannot be employed in every position along the loop), the temperature dependence of the oxygen activity at constant composition must be known. Equivalently, the oxygen activity at the temperature of the measurement can be converted into a molar or mass concentration from which the oxygen activity at the temperature of interest can be subsequently calculated. A suitable basis for such calculations is Henry's law which predicts a linear relationship between the activity of a solute in a (ideally) diluted solution and the solute concentration. The factor of proportionality is the inverse value of the oxygen saturation concentration ($x_{O;S}$ or $c_{O;S}$) as expressed by

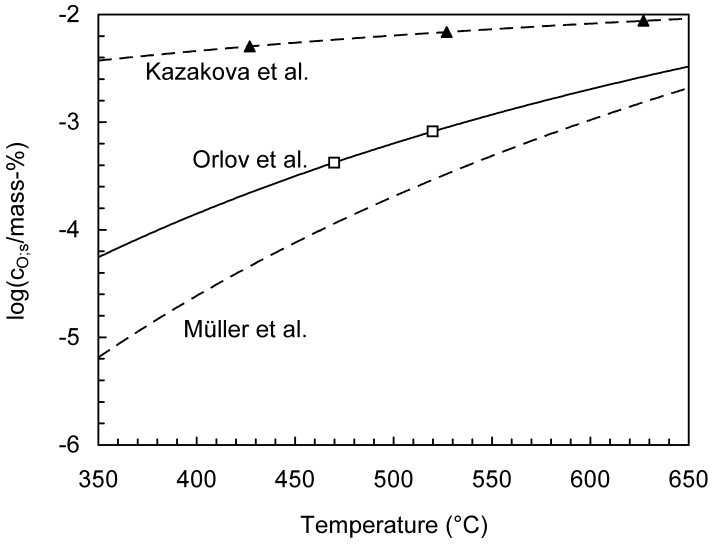

Figure 8 – *Data for the saturation concentration of oxygen in liquid LBE found in the technical literature. In the work of Kazakova et al., the Pb content of the employed Pb-Bi alloy was 43.5 mass-%.*

$$\frac{c_O}{c_{O;s}} \approx \frac{x_O}{x_{O;s}} = \frac{x_{PbO}}{x_{PbO;s}} = a_{PbO} \qquad (2)$$

(x_O: molar concentration of oxygen). Since the oxygen saturation is determined by the precipitation point of the most stable oxide of the liquid-metal components, i.e., PbO in the case of LBE, the lead oxide activity, a_{PbO}, has to be regarded in Equation (2) (analogously to the situation in liquid sodium [10]). a_{O_2} can be converted into a_{PbO} using

$$\log(a_{PbO}) = \log(a_{Pb}) + \frac{1}{2}\log(a_{O_2}) + \frac{11{,}449}{T/(K)} - 5.220 \qquad (3)$$

where the last two terms on the right hand side follow from thermodynamic data for the Pb/PbO equilibrium taken from the database of the software HSC [11].

A major problem with estimating oxygen concentrations in LBE on the basis of Henry's law arises from the very limited and contradictory experimental data on the saturation concentration. Experimental data for $c_{O;s}$ is known from Kazakova et al. (extraction of oxygen as CO/CO_2 from saturated LBE) [12] and Orlov et al. [13], and plotted in Figure 8 as solid triangles and open squares, respectively. When extrapolating the data sets using

$$\log(c_{O;s}) = A - \frac{B}{T/(K)} \qquad (4)$$

the values for $c_{O;s}$ at 550°C differ by approximately half an order of magnitude (Table 3); this deviation can probably not be explained with the fact that Kazakova et al. used an Pb-Bi alloy with 43.5 mass-% Pb instead of the exact eutectic composition [12]. Müller et al. [14] derived the equation

Table 3 – *Saturation concentration of oxygen in liquid LBE at 550°C from extrapolation of experimental data of Kazakova et al. and Orlov et al. and according to the modelling by Müller et al.*

	Kazakova et al.	Orlov et al.	Müller et al.
$c_{O;s}$ (mass-%)	7.30×10^{-3}	1.17×10^{-3}	4.84×10^{-4}

$$\log\left(c_{O;s}/(\text{mass-}\%)\right) = 2.52 - \frac{4803}{T/(K)} \qquad (5)$$

for the solubility of oxygen in liquid LBE by assuming that the solubility in binary Pb-Bi alloys can be modelled on the basis of the solubility in liquid Pb and Bi. The predictions of Equation (5) are also shown in Figure 8 and Table 3.

For consistency with the other parts of this study, Equation (5) is used for estimating the oxygen mass concentration in the LBE. When characterising the testing conditions, the oxygen activity in terms of a_{PbO} – as following from the sensor signals and Equations (1) and (3) – is also mentioned, in order to give a (thermodynamic) measure for the oxygen content which is independent from the uncertainties discussed above.

2.4.2 Oxygen content in the course of the experiments

Considering future applications of molten LBE as a process medium, the oxygen content should be high enough to allow for the oxidation of steels, but significantly below the threshold for the precipitation of oxides of Pb and Bi. If the first criterion is not fulfilled, the steels will be prone to dissolution in the LBE and a satisfactorily life-time of the plant components cannot be expected; but if the oxygen content is too high, the proper operation of the plant is at risk from plugging of the flow paths. For the experiments in the CORRIDA loop, an oxygen concentration around 10^{-6} mass-% was specified, so that, according to calculations by Müller et al. [14], both criteria are fulfilled for the whole range of temperatures prevailing in the CORRIDA loop (380°-550°C).

At the onset of operating the loop, it was assumed that oxygen transfer between the oxygen-containing gas stream and the LBE in the OCB is sufficiently fast and, in the steady state, the exchanged mass is low, so that chemical equilibrium between the gas and the liquid metal is achieved without significantly altering the gas composition. Based on these assumptions and the specified oxygen mass concentration, an oxygen partial pressure of 1.30×10^{-23} bar (1.30×10^{-18} Pa) at 550°C (operating temperature of the OCB) was chosen for the gas stream introduced into the OCB. This partial pressure corresponds to a H_2-to-H_2O ratio of 0.04 in the gas which was realised by humidifying an Ar-0.03 vol.-% H_2 mixture at 4°C. The volume flow of gas was 500 standard-cm³/min.

Figure 9 shows a plot of the EMF measured with the oxygen sensors during the first 5000 h of effective operation of the CORRIDA loop and the oxygen activity (in terms of a_{PbO}) and oxygen concentration which result from the signal of the Pt/air sensor at the inlet of the first test-section. Although the oxygen-containing gas stream which

was introduced into the OCB met the specifications quite well [8], the oxygen activity in the LBE fell below the target value already after approximately 100 h of operation. In the following, the decrease of the oxygen activity in the LBE slowed down, but the oxygen up-take from the gas phase was still not sufficient to compensate for the oxygen consumption due to the oxidation of the steel specimens in the test-sections and especially of the construction material of the loop. Only after a maintenance interval (involving emptying and refilling of the loop) which became necessary after approximately 1000 h, an oxygen activity in the range of the target value was achieved (Figure 9).

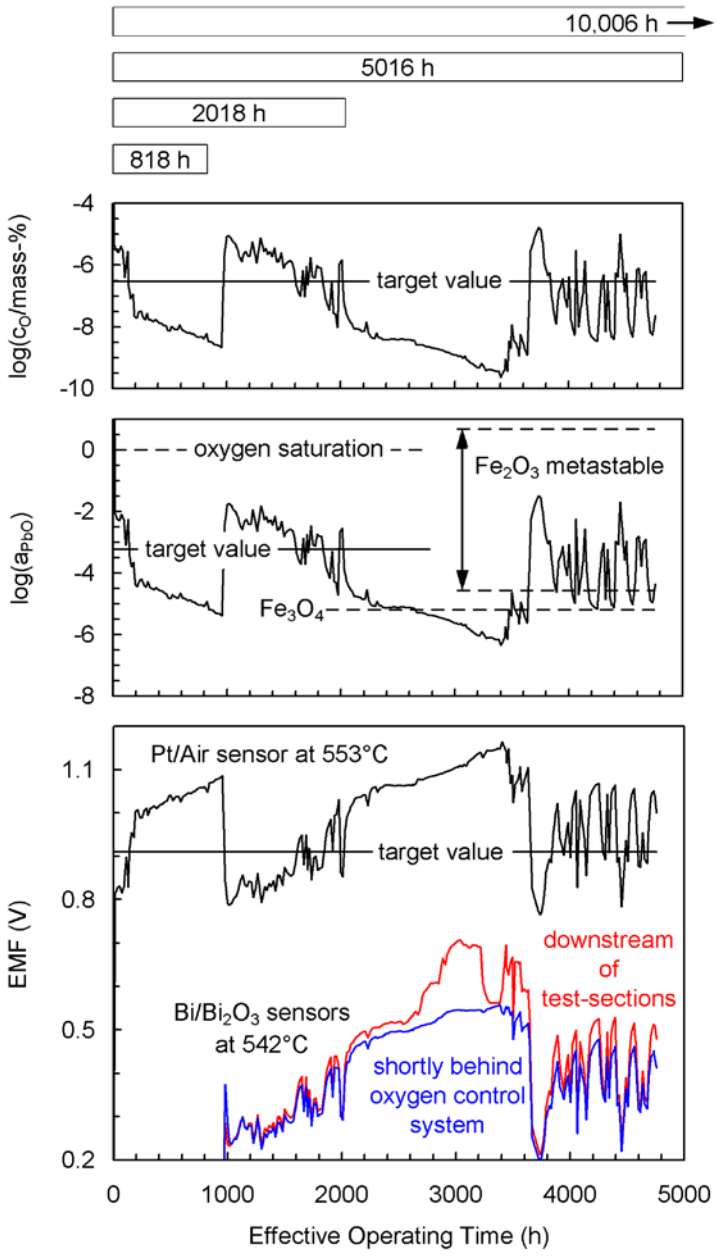

Figure 9 – *Record of electromotive forces (EMF) measured with oxygen sensors during the first 5000 h of effective operation of the loop. The EMF indicated by the Pt/air sensor which resides near the inlet of the first test-section (at 553°C) was converted into activity of PbO, a_{PbO}, and oxygen concentration according to Equation (5). The bars at the top of the figure indicate periods of exposure of*

P122 and ODS.

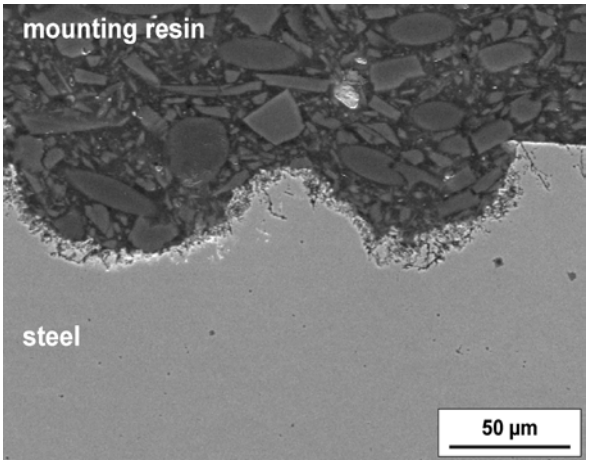

Figure 10 – *Local dissolution of a specimen of the construction material of the loop (DIN W.-Nr. 1.4571) after exposure for 1200 h at 550°C and very low oxygen content ($c_O < 5\times10^{-9}$ mass-%; $a_{PbO} < 10^{-5}$). Adherent corrosion products and LBE were removed in half-concentrated nitric acid.*

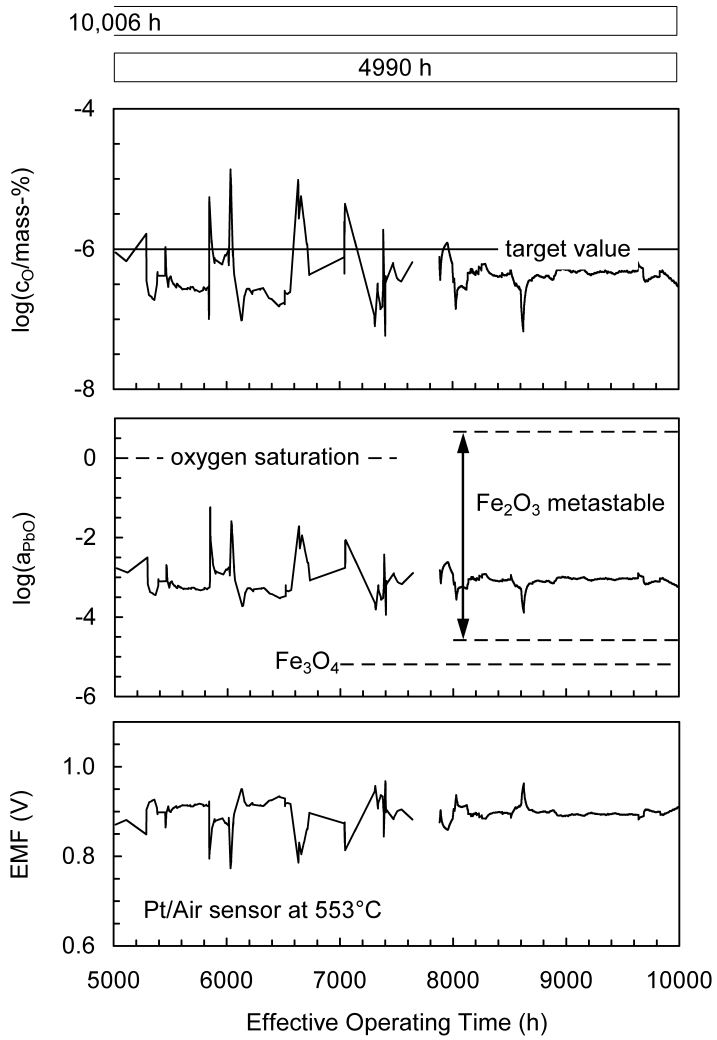

Figure 11 – *Record of the electromotive force (EMF) measured with the Pt/air sensor near the inlet of the first test-section between 5000 and 10,000 h of effective operation of the loop. The EMF was converted into activity of PbO, a_{PbO}, and oxygen concentration according to Equation (5). The bars at the*

top of the figure indicate periods of exposure of P122 and ODS.

After resuming operation, the oxygen activity decreased again, more slowly than during the first operation period but steadily. Between 2300 h and 3500 h of effective operation, the oxygen activity in the LBE was in the range and below the minimum necessary for formation of magnetite, Fe_3O_4, i.e., conditions favourable for Fe dissolution and therefore dissolving corrosion of steels arose. A specimen of the construction material of the loop (DIN W.-Nr. 1.4571) which was exposed in one of the test-sections only during this period of operation showed indeed dissolving corrosion (Figure 10), giving evidence that the much too low oxygen activity was not pretended by malfunction of the oxygen sensors. The significant deviation of the EMF indicated by the Bi/Bi_2O_3 sensor which is positioned downstream of the test-sections (Figure 9 red curve) from the signal of the Bi/Bi_2O_3 sensor shortly behind the OCB (Figure 9 blue curve) probably results from the influence of dissolved metals which are less-noble than Pb on the oxygen activity in the LBE, i.e., such solutes may lower the oxygen activity for constant oxygen concentration (which questions the practical applicability of the method for estimating oxygen concentrations in LBE discussed in the previous sub-section).

The experience from the first 3500 h of operation showed, that the oxygen partial pressure in the gas introduced into the OCB has to be much higher than the equilibrium partial pressure which corresponds to the designated oxygen activity in the LBE. In the following, compressed air was periodically added to the gas stream by which the oxygen activity in the LBE was raised to the target value when the threshold for Fe_3O_4 stability had been approached in consequence of oxygen consumption in the loop (Figure 9; operating time >3500 h). After 5000 h of effective operation, the oxygen control system has been supplemented by a precision valve which allows for the introduction of a finely adjusted, continuous air stream (~0.3 cm³/min) in addition to humidified Ar (~500 cm³/min). Thus, the oxygen activity in the LBE was kept in a sufficiently narrow range around the target value during the next 5000 h of operation (Figure 11).

2.4.3 Summary of the testing conditions

Table 4 summarises the exposure conditions for P122, ODS and the GESA-treated steels.

P122 and ODS were exposed in the CORRIDA loop for 818, 2018, 4990 and 10,006 h. In the case of both steels, the exposure for 4990 h was performed at an approximately constant and comparatively high oxygen activity in the LBE which corresponds to 5×10^{-7} mass-% ($a_{PbO} = 10^{-3}$). For the other exposure times, the conditions with respect to the oxygen content of the LBE significantly varied according to Figure 11. The specimens exposed for 10,006 h faced varying conditions during the first 5016 h, followed by a period of 4990 h with permanently high oxygen activity around $a_{PbO} = 10^{-3}$.

The specimens of the steels which were partly surface-alloyed with aluminium were exposed for 818, 2018 and 5016 h to varying conditions with respect to the oxygen content of the LBE. An experiment for nominally 10,000 h is still going on and is planned to be terminated in November 2005. The respective specimens will then have experienced a permanently high oxygen activity in the range of $a_{PbO} = 10^{-3}$. Ad-

ditional information on the long-term behaviour of P122 and ODS under such conditions will be retrieved from the reverse side (non-aluminised part) of those specimens.

Table 4 – *Summary of the exposure conditions.*

P122 and ODS (without GESA-treatment)

duration (h)	composition of LBE (mass-%)			
	Pb	Bi	O	a_{PbO}
818	46 (a_{Pb}=0.370)	54 (a_{Bi}=0.462)	$5\times10^{-9} \le c_O \le 5\times10^{-6}$	$10^{-5} \le a_{PbO} \le 10^{-2}$
2018			$5\times10^{-9} \le c_O \le 5\times10^{-6}$	$10^{-5} \le a_{PbO} \le 10^{-2}$
4990			$\sim5\times10^{-7}$	$\sim10^{-3}$
10,006			$5\times10^{-10} \le c_O \le 5\times10^{-6}$ last 4,990 h: $\sim5\times10^{-7}$	$10^{-6} \le a_{PbO} \le 10^{-2}$ last 4,990 h: $\sim10^{-3}$
temperature: 550° ± 2°C				
flow velocity: 2 ± 0.2 m/s				

GESA-treated steels

duration (h)	composition of LBE (mass-%)			
	Pb	Bi	O	a_{PbO}
818	46 (a_{Pb}=0.370)	54 (a_{Bi}=0.462)	$5\times10^{-9} \le c_O \le 5\times10^{-6}$	$10^{-5} \le a_{PbO} \le 10^{-2}$
2018			$5\times10^{-9} \le c_O \le 5\times10^{-6}$	$10^{-5} \le a_{PbO} \le 10^{-2}$
5016			$5\times10^{-10} \le c_O \le 5\times10^{-6}$	$10^{-6} \le a_{PbO} \le 10^{-2}$
temperature: 550° ± 2°C				
flow velocity: 2 ± 0.2 m/s				

The temperature and flow velocity of the LBE were 550° ± 2°C and 2 ± 0.2 m/s, respectively. Although the oxygen content temporarily was significantly lower than initially planned in the experiments with varying oxygen content, all these exposures started at high oxygen activity.

2.5 Post-test examinations

After removal from the CORRIDA loop, three circular slices – two with a thickness of ~2 mm and a third with a thickness of ~10 mm – were cut from each of the corroded specimens (Figure 12). The thin slices were prepared for examination in cross section using light- and electron-optical methods supplemented by energy-dispersive X-ray micro-analyses (EDX). Wavelength-dispersive electron-probe micro-analyses (EPMA) were performed with selected cross-sections. The thick slice was further cut longitudinally and, from one half, a longitudinal cross-section was prepared for examination in the scanning electron microscope (SEM) and with EDX. For selected specimens, the second half the thicker slice was rinsed in hot fat (at ~180°C) so as to

remove residual LBE from the surface and access solid corrosion products (oxides) on the steel surface for analysis via X-ray diffraction (XRD).

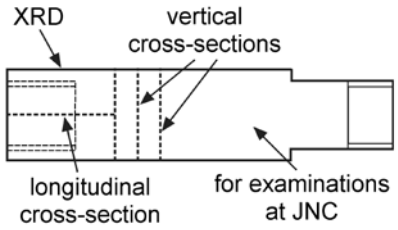

Figure 12 – *Illustration of the fragmentation of specimens for the post-test examinations.*

The remaining part of the specimens was retained for investigations performed at JNC.

3 Results and Discussion

3.1 P122

3.1.1 Oxidation behaviour at 550°C and $c_O \approx 5\times10^{-7}$ mass-% ($a_{PbO} \approx 10^{-3}$)

The oxide scales which were observed on the surface of P122 after exposure for 4990 h to flowing LBE at 550°C and $c_O \approx 5\times10^{-7}$ mass-% ($a_{PbO} \approx 10^{-3}$) are shown in Figures 13 and 14. Figure 13 is representative for domains with a continuous scale of non-uniform thickness. A qualitative EDX-linescan along this scale revealed that the main part consists of an Fe-Cr mixed-oxide (Figure 13 bottom), i.e., (Fe,Cr) spinel according to the XRD-spectrum recorded from the surface of the oxide scale after removal of adherent LBE (Figure 15). An internal oxidation zone (IOZ) which has formed via diffusion of oxygen into the steel (especially along grain boundaries) is mostly present beneath the spinel layer and consists of Cr-rich oxide precipitates in the metallic matrix. The oxide which precipitates in the steel can either be a Cr-rich spinel (M_3O_4), a Cr-rich mixed-oxide of type α-M_2O_3 or chromia, α-Cr_2O_3. The EDX-linescan in Figure 13 also shows a Cr-depleted zone of ~2 µm in the steel at the interface with the IOZ and inclusions of Cu-rich metallic particles in the spinel layer.

Domains with a continuous spinel layer alternate with sites where the spinel layer is interrupted by regions consisting of Cr-depleted steel, which resulted from pronounced non-uniform inward-growth of the oxide scale. Around such peaks in the instantaneous surface-profile of the steel, parts of the spinel layer can be missing, most likely due to spalling during the exposure. After partial spalling of the spinel, the Cr-depleted peaks in the steel surface also exceed the surface of the adherent part of the oxide scale and were thus detected by the XRD-spectrum recorded from the oxidised surface (Figure 15; signals accounting for Fe). The area ratio of domains exhibiting an interrupted spinel layer to sites where this layer is continuous is approximately 1:5 (in the examined vertical cross-sections).

As a basis for quantifying the metal recession (material consumption) in the course of oxidation, the thickness of the oxide scale was measured in a light-microscope at magnification 500× at 12 sites uniformly distributed along the circumference of the

specimen (vertical cross-section). Sites where partial spalling of the spinel layer was evident were neglected in these measurements. The mean overall thickness of the

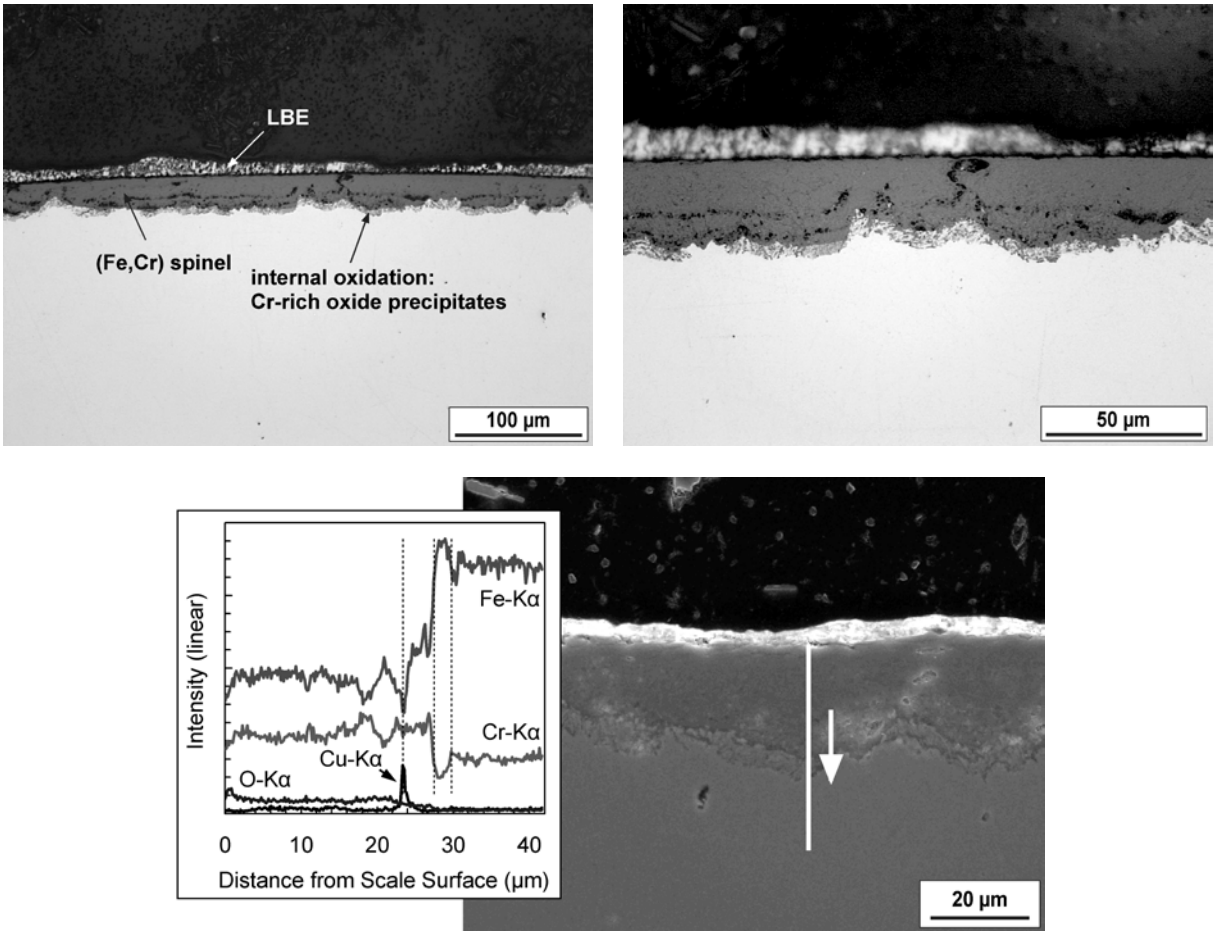

Figure 13 – *Oxide scale on the surface of P122 after exposure to flowing LBE at 550°C and $c_O \approx 5\times10^{-7}$ mass-% ($a_{PbO} \approx 10^{-3}$) for 4990 h. Top: light-optical micrographs of a vertical cross-section. Bottom: electron-optical micrograph of a longitudinal cross-section and qualitative EDX-linescan.*

scale and the mean thickness of the spinel layer and IOZ are shown in Figure 16. For the estimation of a mean corrosion rate, it was assumed that the instantaneous position of the surface of the inward-growing spinel layer approximately coincides with the original position of the steel surface, which follows from exposure experiments performed in flowing liquid Pb with steels partly surface-alloyed with aluminium [15]. The resulting linear oxidation rate is 0.05 mm/y with an uncertainty of ±20% which follows from the maximum and minimum deviation of the single measurements from the mean value (Figure 16). However, it should be noted that the mean oxidation rate was determined using an arbitrarily chosen cross-section and more or less significant deviations from the stated value may occur in other locations along the specimen. A site where the local metal recession was obviously higher than in the investigated cross-section (~0.08 mm/y) was observed in the examined longitudinal cross-section, in the vicinity of a Cr-depleted peak in the steel surface (Figure 14 bottom).

No Fe-oxide was found on the surface of the oxide scale although the oxygen content, i.e., the oxygen activity in the LBE, apparently was always high enough for the

formation of magnetite, Fe_3O_4. The thermodynamic stability of Fe_3O_4 indicated in Figure 11 (middle), however, refers to the formation from pure metallic Fe with activi-

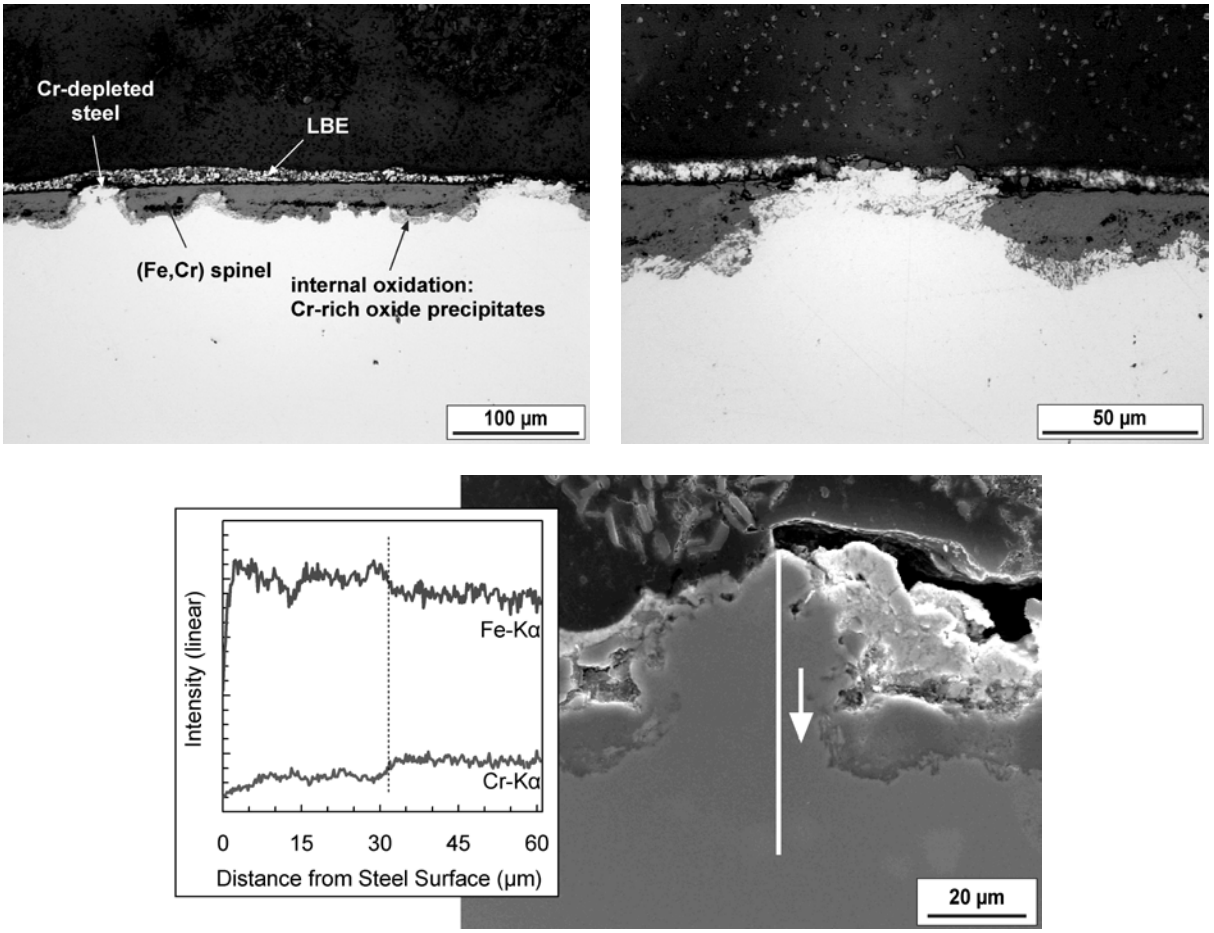

Figure 14 – *Cr-depleted peaks in the instantaneous surface of P122 after exposure to flowing LBE at 550°C and $c_O \approx 5\times10^{-7}$ mass-% ($a_{PbO} \approx 10^{-3}$) for 4990 h. Top: light-optical micrographs of a vertical cross-section. Bottom: electron-optical micrograph of a longitudinal cross-section and qualitative EDX-linescan. The local metal recession estimated from this micrograph is ~45 µm after 4990 h.*

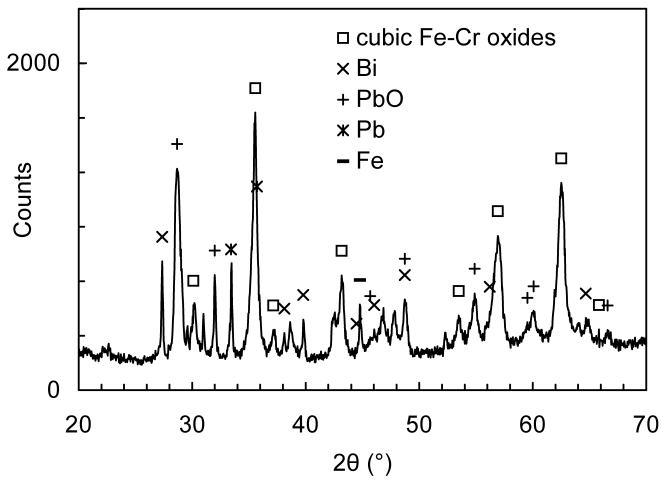

Figure 15 – *XRD-spectrum recorded from the surface of P122 after exposure to flowing LBE at 550°C and $c_O \approx 5\times10^{-7}$ mass-% ($a_{PbO} \approx 10^{-3}$) for 4990 h. Adherent LBE was removed by rinsing in hot fat. Cubic Fe-Cr oxides can be magnetite, Fe_3O_4, (Fe,Cr) spinel, $FeCr_2O_4$, or maghaemite, γ-Fe_2O_3. γ-Fe_2O_3 is only metastable under the exposure conditions.*

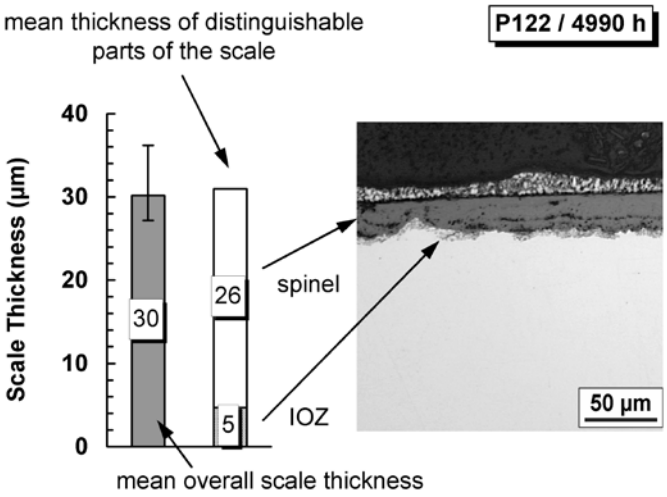

Figure 16 – *Mean thickness of the oxide scale on the surface of P122 after exposure to flowing LBE at 550°C and $c_O \approx 5\times10^{-7}$ mass-% ($a_{PbO} \approx 10^{-3}$) for 4990 h. The error bar indicates the deviation of the maximum and minimum, respectively, of 12 measurements from the mean value.*

ity $a_{Fe} = 1$. As long as the Fe content of the LBE is below the respective saturation concentration (which is likely at the highest temperature in a non-isothermal LBE loop), the Fe activity (with reference to pure Fe) at the LBE/oxide scale (spinel) interface is less than unity so that, considering this location, an oxygen activity higher than following from Figure 11 is necessary for the formation of Fe_3O_4. Accordingly, Fe which diffused through the spinel layer was dissolved in the LBE and did not form Fe-oxide on the oxide scale surface. Further explanations for the absence of Fe_3O_4 might be erosion of the outward-growing Fe-oxide by the flowing LBE, possibly already in *statu nascendi* (immediately after nucleation) or spalling of the Fe-oxide. But at least in the latter case some remnants of Fe_3O_4 should have been found on the oxide scale surface.

The prove for Fe transport through the spinel layer is indirect and follows from the inward-growth of this layer (which is evident from the irregular profile of the interface between the oxide scale and the steel, e.g., in Figure 13). Considering that the Pilling-Bedworth ratio for the formation of Fe-Cr oxides of type M_3O_4 (spinel, magnetite) from (ferritic) steel is ~2 [16], the volume of the inward-growing (Fe,Cr) spinel amounts approximately twice the volume of P122 consumed by spinel formation. This means that either the whole spinel layer is lifted (cracks and spalls off) due to continuing spinel formation at the oxide scale/steel interface or a significant part of steel constituents diffuses through the spinel layer and is removed from the scale surface, e.g., by dissolution in the flowing LBE. From the main constituents of P122 (Fe and Cr), the less-noble Cr probably is comparatively immobile in the oxide phase and preferably remains in the spinel layer and the IOZ (within the original limits of the steel), so that primarily Fe diffuses through the spinel layer [17]. The higher affinity of Cr to oxygen becomes manifest also in the Cr-depletion of the steel beneath the

spinel layer and the IOZ (Figure 13 bottom). When the surface of the spinel layer remains in the original position of the steel surface, approximately half of the mass of steel consumed in the oxidation process gets lost after diffusion (of Fe) through the spinel layer.

3.1.2 Behaviour under varying conditions with respect to the oxygen content

Figure 17 and 18 show the oxide scales which formed on the surface of P122 in the course of the exposure experiments for 818 and 2018 h, respectively. In these experiments, the oxygen content of the LBE varied between 5×10^{-9} and 5×10^{-6} mass-% ($10^{-5} \leq a_{PbO} \leq 10^{-2}$) according to Figure 9. Under these conditions, the formation of (Fe,Cr) spinel sets in locally, and lateral growth (parallel to the steel surface) starting from the nucleation sites results in a continuous layer with non-uniform thickness. Beneath the spinel, oxygen diffuses into the steel and causes precipitation of Cr-rich oxides (Cr-rich spinel, a Cr-rich α-M_2O_3 or chromia) within the steel. This internal oxidation seems to start not until the spinel has reached a thickness between 5 and 7 µm. After the shorter exposure time (816 h), the Cr-rich precipitates are of small size and uniformly dispersed in the metallic matrix (Figure 17); at the IOZ/steel inter-

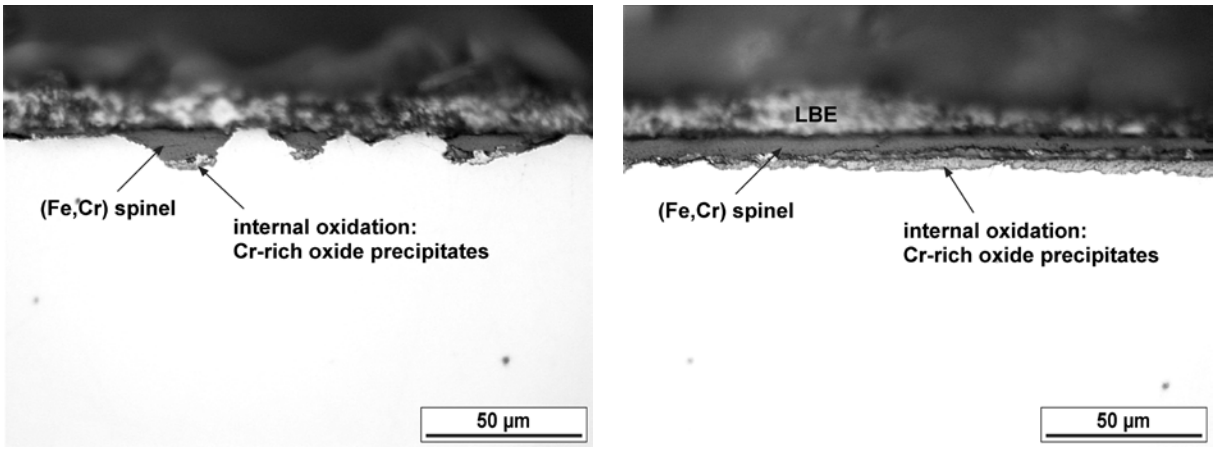

Figure 17 – *Oxide scale on the surface of P122 after exposure for 818 h to flowing LBE at 550°C. The oxygen concentration in the LBE varied between 5×10^{-9} and 5×10^{-6} mass-% ($10^{-5} \leq a_{PbO} \leq 10^{-2}$). Left: domain with local spinel formation. Right: continuous spinel layer and internal oxidation accompanied by the precipitation of small, Cr-rich oxide particles which are uniformly dispersed in the steel matrix. Note the inward-growth of the spinel which is evident from the left micrograph.*

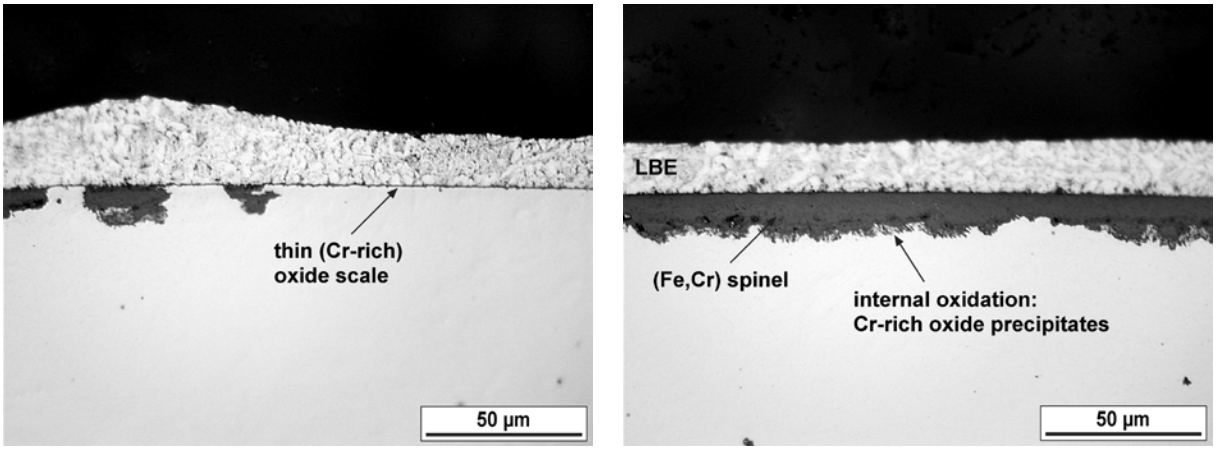

Figure 18 – *Oxide scale on the surface of P122 after exposure for 2018 h to flowing LBE at 550°C. The oxygen concentration in the LBE varied between 5×10^{-9} and 5×10^{-6} mass-% ($10^{-5} \leq a_{PbO} \leq 10^{-2}$). Left: domain with a thin, protective scale and local spinel formation. Right: continuous spinel layer and internal oxidation along grain boundaries of the steel. Note the inward-growth of the spinel which is evident from the left micrograph.*

face, a thin continuous layer of Cr-rich oxide has formed. With increasing exposure time, the initially formed IOZ is at least partially consumed by inward-growth of spinel, and a second stage of internal oxidation starts resulting in coarser Cr-rich oxide particles along the grain boundaries of the steel (Figure 18). Such a coarsened IOZ is not always present. After both exposure times, domains which are protected from significant oxidation (scale thickness <1 µm) by a thin, Cr-rich oxide scale which most likely consists of an oxide of type α-M_2O_3 were found (e.g., Figure 18 left).

A more detailed discussion of the results of the exposure experiments for 818 and 2018 h can be found in Reference 8.

For comparing the oxidation behaviour of P122 under varying conditions with respect to the oxygen content and at $c_O \approx 5\times10^{-7}$ mass-% ($a_{PbO} \approx 10^{-3}$) in exposure experiments which lasted for about the same time, the reverse side (non-aluminised part) of a GESA-treated specimen which was exposed for 5016 h at oxygen contents between 5×10^{-10} and 5×10^{-6} mass-% ($10^{-6} \leq a_{PbO} \leq 10^{-2}$) is included in the analysis. The reverse side of GESA-treated specimens of P122 differed from the specimens of P122 in the surface state (ground surface and surface finished by turning). The influence of the surface-finish on the oxidation should be mainly restricted to the short-term behaviour, unless the formation of a very stable, protective scale which survives (most of) the exposure period is promoted. Comparing the reverse side of GESA-treated specimens exposed for 818 and 2018 h with P122 after the same exposure times (identical conditions with respect to the oxygen content), the ground surface on the reverse side of GESA-treated specimens exhibits a significantly less tendency to form a thin Cr-rich scale. In other words, the surface-finish by turning favours the formation of this protective type of scale, most likely because a higher degree of surface deformation enhances Cr-diffusion to the surface [18]. Considering that the spinel layer growth comparatively fast inwards, the influence of the surface-finish of the steel should be less pronounced, so that, in this regard, the non-aluminised part of GESA-treated specimens at least qualitatively behaves in a fashion similar to P122 with a turned surface.

As shown in Figure 19, a continuous oxide scale with a slightly non-uniform oxide scale/steel interface formed on the reverse side of GESA-treated P122 in the course of the exposure for 5016 h to varying conditions with respect to the oxygen content. According to qualitative EDX-analyses performed along this scale (Figure 19 bottom), the inner part is significantly enriched in Cr and the outer (more Fe-rich) part exhibits a composition comparable to the spinel layer observed on P122 after exposure for 4990 h at permanently high oxygen content of the LBE (Figure 13 bottom). Thus, it seems that the composition of the inner part of the oxide scale is significantly influenced by the varying conditions (mostly low oxygen activity and, therefore, enrichment of less-noble Cr in this part of the scale), while the outer part is not. These finding basically reflects the specific mechanism of spinel growth in oxygen-containing flowing LBE, i.e., all the Cr is oxidised within the original limits of the steel (after inward-diffusion of oxygen) and Fe partially leaves the inward-growing oxide scale (after diffusion towards the scale surface) to maintain the volume-balance between ox-

ide formation and consumption of the steel (see previous sub-section, p.17). Oxygen transport in the scale does apparently not limit the inward-growth of the spinel at permanently high oxygen activity and also initially under varying conditions with respect to the oxygen content (otherwise, internal oxidation could not occur), so that

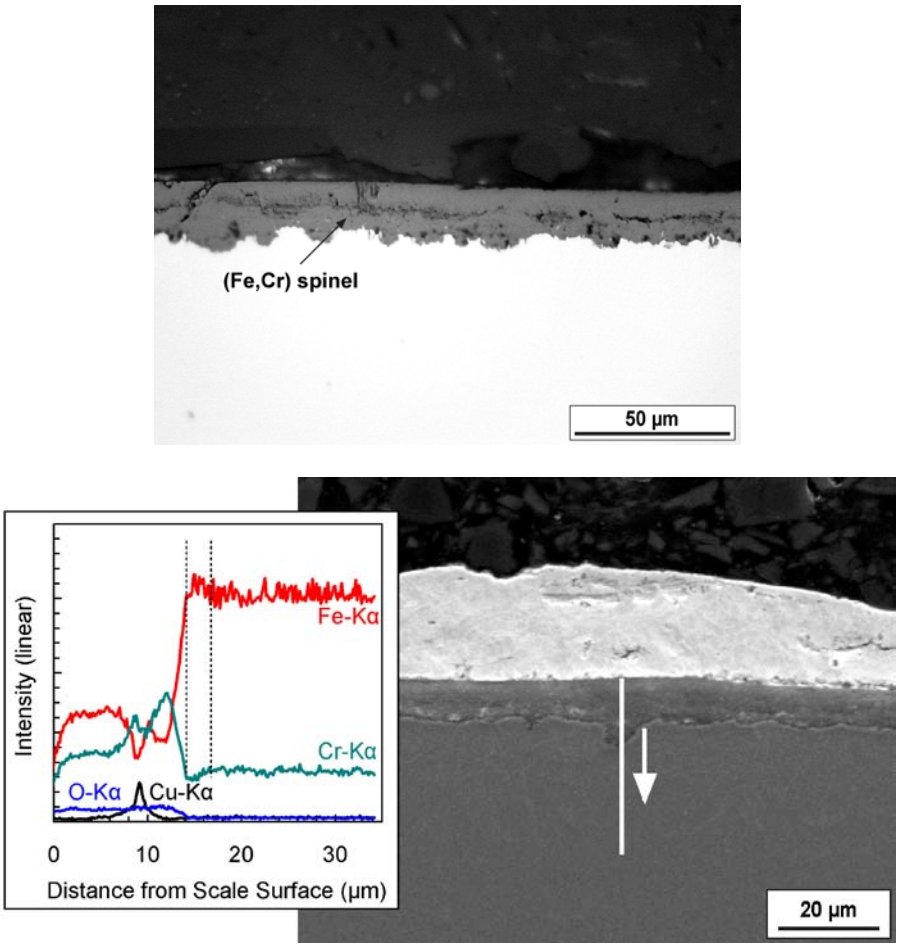

Figure 19 – *Oxide scale on the surface of P122 after exposure for 5016 h to flowing LBE at 550°C (non-aluminised part of GESA-treated specimen). The oxygen concentration in the LBE varied between 5×10^{-10} and 5×10^{-6} mass-% ($10^{-6} \leq a_{PbO} \leq 10^{-2}$). Top: light-optical micrograph of continuous spinel layer. Bottom: electron-optical micrograph and qualitative EDX-linescan of the spinel layer.*

the composition of the steel rather than the oxygen activity in the LBE determined the Fe-to-Cr ratio in the spinel. Considering that only the inner part of the scale showed a significant enrichment in Cr after the exposure to varying conditions, changes in the oxide composition induced by a decreasing oxygen activity in the LBE start at the oxide scale/steel interface, where the oxide continues to grow. For this change in composition to proceed in the direction of the scale surface, Cr has to be transported through this Cr-rich part and displaced Fe must diffuse simultaneously to the scale surface. The first of these sub-processes is probably slow so that the Fe-to-Cr ratio in the outer part of the scale remains unaffected for some time. Slight internal oxidation locally occurred beneath the Cr-rich oxide which, in this case, probably is a Cr-rich spinel rather than Cr-rich α-M_2O_3.

The pronounced (Cr-depleted) peaks in the instantaneous surface-profile of the steel, the development of which is accompanied by partial spalling of the spinel layer (Figure 14), were not observed after exposure for 5016 h under varying conditions with respect to the oxygen content (reverse side of GESA-treated specimen). Since the difference in the local velocity of oxide growth is more pronounced between the thin protective scale and inward-growing spinel, the surface-finish of the specimens compared probably was more decisive in this regard than the mostly lower oxygen content of the LBE during the exposure for 5016 h. This feature of the oxidation of P122 in flowing LBE was also observed on the specimen with a turned surface which was exposed for 10,006 h, 5016 h at varying (mostly low) oxygen content and another 4990 h at $c_O \approx 5\times10^{-7}$ mass-% (Figure 20). Domains with a continuous spinel layer where spalling did apparently not occur are the exception in the case of this specimen (Figure 21). For both the spinel layer and remnants after partial spalling, the oxide at the interface with the steel is enriched in Cr, which, as aforementioned, may be an effect of periods of low oxygen content of the LBE in the course of the first half of the exposure.

Looking closer at the continuous scale after exposure for 10,006 h (Figure 21), also the non-uniformity of the thickness of the spinel layer itself increased after additional 4990 h at high oxygen content of the LBE (Figure 19). This implies that some parts

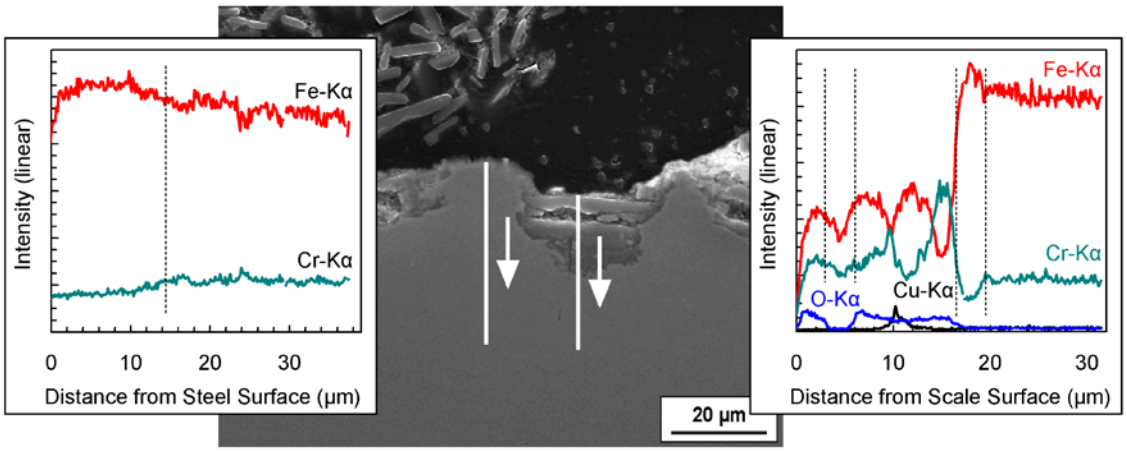

Figure 20 – *Cr-depleted peaks in the instantaneous steel surface and partially spalled spinel layer after exposure of P122 for 10,006 h to flowing LBE at 550°C. The oxygen concentration in the LBE*

varied between 5×10^{-10} and 5×10^{-6} mass-% ($10^{-6} \leq a_{PbO} \leq 10^{-2}$) with the oxygen content being in the range of 5×10^{-7} mass-% ($a_{PbO} \approx 10^{-3}$) during the last 4990 h of exposure. Top: light-optical micrograph. Bottom: electron-optical micrograph and qualitative EDX-linescan of a peak in the steel surface (left) and remnants of the spinel layer.

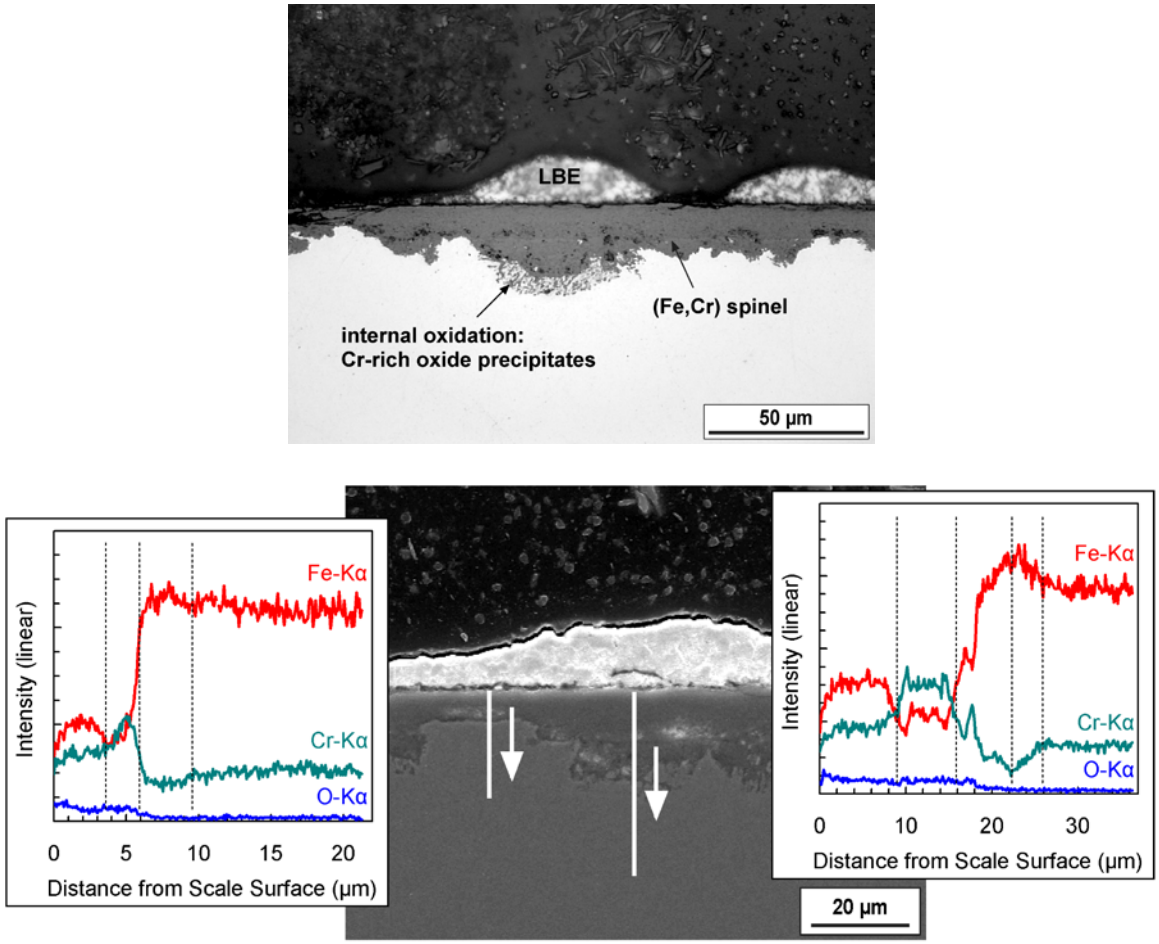

Figure 21 – *Domain with continuous oxide scale on the surface of P122 after exposure for 10,006 h to flowing LBE at 550°C. The oxygen concentration varied between 5×10^{-10} and 5×10^{-6} mass-% ($10^{-6} \leq a_{PbO} \leq 10^{-2}$) and was ~$5\times10^{-7}$ mass-% ($a_{PbO} \approx 10^{-3}$) during the last 4990 h of the exposure experiment. Top: light-optical micrograph of continuous spinel layer. Bottom: electron-optical micrograph and qualitative EDX-linescan of thinner (left) and thicker parts of the oxide scale.*

of the scale which established during the first 5016 h at mostly low oxygen content of the LBE are a more efficient barrier for diffusion of oxygen to the oxide scale/ steel interface than others. Considering the results of qualitative EDX-analyses along the scale after the exposure for 10,006 h, an exceptionally Cr-rich oxide, possibly of type α-M_2O_3, may have formed locally at this interface indicated by the comparatively narrow peak in the curve representing the distribution of Cr in the thinner parts of the scale (left EDX-linescan in Figure 21; the height of this peak is reduced due to the limited spatial resolution of EDX measurements). In contrast to this, the thicker parts of the scale (right EDX-linescan in Figure 21) show a broader distribution of Cr in the scale indicating that some inward-growth occurred after the Cr-enrichment at an interim interface with the steel. In this case, the local Cr-supply which depends on the distribution of Cr in the steel probably was too low to establish the exceptionally Cr-rich oxide observed beneath the thinner parts of the spinel layer. Instead, the com-

paratively slight Cr-enrichment may have resulted only in the formation of a Cr-rich spinel which continued to grow especially after the increase of the oxygen content of the LBE. An internal oxidation zone of significant thickness which is another indication for oxygen transport through the scale was observed mostly beneath thicker parts of the scale after the exposure for 10,006 h.

However, one of the most important findings of the experiments under varying conditions with respect to the oxygen content of the LBE is that no liquid metal corrosion occurred even if the oxygen content was temporarily in the range of 5×10^{-10} mass-% ($a_{PbO} = 10^{-6}$). But it should be emphasized that all experiments started with high oxygen content of the LBE.

3.1.3 Proposed oxidation mechanism

In the following, the results presented in the previous two sub-sections are summarised in the form of a preliminary oxidation mechanism for P122 in flowing LBE at 550°C, with an emphasis on the evolution of peaks in the instantaneous surface-profile of the steel and potential reasons for partial spalling of the spinel layer around the more-pronounced ones. The latter point is especially important to judge the oxidation behaviour of the steel at times which are not covered by the experiments. A theoretical analysis of the oxidation of binary alloys consisting of a noble and a considerably less noble metal, which was performed by Wagner [19], was used as a basis for the proposed mechanism.

Considering first that the surface of P122 was finished by turning, the initially formed scale consists of a thin, Cr-rich oxide film (probably of type α-M_2O_3) which can protect the steel from significant further oxidation. For reasons discussed in Reference 8, this scale locally breaks down, followed by significantly faster formation of inward-growing (Fe,Cr) spinel which subsequently spreads across the surface. A slight Cr-depletion beneath the spinel (and an internal oxidation zone which is neglected in this discussion) indicates that the inward-growth consumes more Cr than contained in the volume of steel transformed so that a driving force for lateral diffusion of Cr (parallel to the steel surface) arises in the steel where remnants of the protective scale still cover the surface (Figure 22). This lateral Cr-diffusion is responsible for the pronounced Cr-depletion of the peaks in the steel surface which result from the significantly different local oxidation rates beneath the protective scale and where spinel formation initiated.

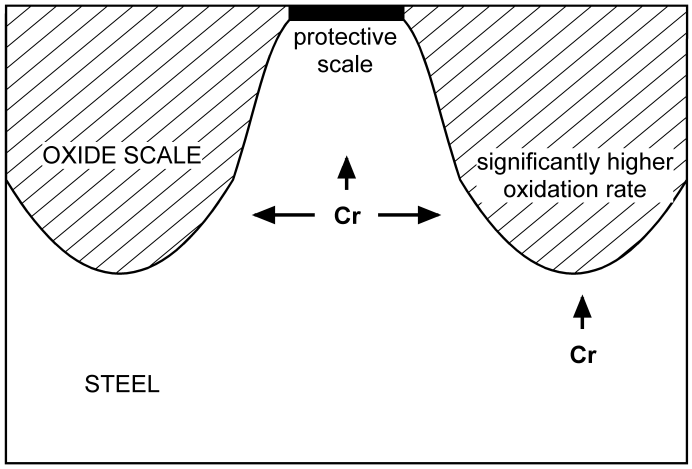

Figure 22 – *Main directions of Cr-transport in P122 beneath remnants of a protective scale.*

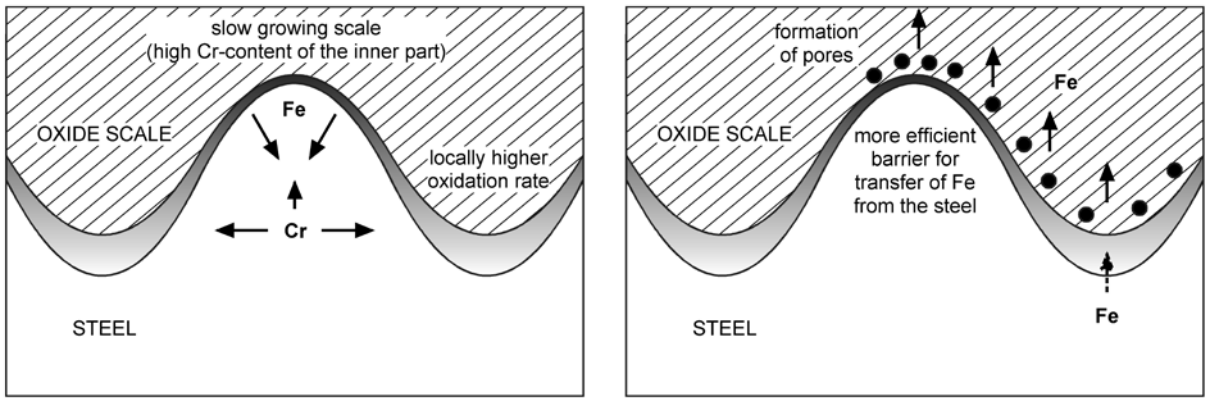

Figure 23 – *Schematic illustration of the main directions of Fe- and Cr-transport after some time of non-uniform oxidation. Left: transport in the steel which results in a significant Cr-depletion of peaks in the instantaneous steel surface. Right: Fe transport in the oxide scale (spinel layer).*

The post-test examinations additionally showed that even if spinel formation started, a Cr-rich and comparatively protective inner part of the scale locally evolves, especially during periods of low oxygen content of the LBE. A heterogeneous distribution of Cr in the steel can be responsible for this kind of behaviour, i.e., an exceptionally Cr-rich oxide (probably also of type α-M_2O_3) forms at the oxide scale/steel interface when this continuously inward-moving interface crosses a Cr-rich domain within the steel. The result with respect to the shape of the instantaneous steel surface and the Cr-depletion of peaks in the surface-profile is qualitatively similar to sites where remnants of the initially formed Cr-rich scale still protect the steel, except for the spinel which grows until the Cr-rich oxide at the interface with the steel has established. A surface-analytical examination on the early stages of the oxidation of T91 performed by Tökei et al. [20] showed that the distribution of Cr in surface oxides qualitatively coincides with the different Cr-content of neighbouring martensite laths in the steel. The influence of other factors like segregation of silicon, phosphorous and nitrogen were also found in this investigation.

The conditions for Fe-transport may be responsible for partial spalling of the spinel layer around the Cr-depleted peaks in the steel surface, as illustrated in Figure 23 for the more general case that only the inner part of the scale is Cr-rich. Considering the inside of a peak, diffusion of Cr (perpendicular and especially parallel to the steel surface) towards the oxide scale/steel interface leaves behind vacancies in the steel grains and at grain boundaries which can be refilled by Fe diffusion from the surface into the bulk of the peak (Figure 23 left). The inward-diffusion of Fe produces pores at the oxide scale/steel interface which may not be filled by inward-growing oxide due to insufficient supply of oxygen beneath the Cr-rich part of the scale. The accumulation of pores at this interface can result in local detachment and spalling after release of growth-stresses in the scale. On the other hand, there is a driving force for Fe transport to the scale surface as was discussed on p. 17. When Cr-rich oxides establish at the oxide scale/steel interface, the supply of Fe from the steel is significantly reduced and pores are likely to occur in the spinel layer, especially above the Cr-rich parts of the scale (Figure 23 right). If the Fe concentration (activity) in the bulk of the spinel is determined by the mean composition of the steel and independent from the oxide scale thickness, the activity gradient responsible for Fe transport will be the steeper the thinner the scale. Additionally, residual supply of Fe from the steel is lower where the inner part of the scale is especially Cr-rich. Thus, partial spalling subsequent to accumulation of pores in the spinel layer is likely to start at the peaks in the steel surface and should be the more pronounced the higher the oxygen content of the LBE (low Fe activity at the oxide surface). Where the initially formed, Cr-rich oxide still covers the surface (no spinel formation), partial spalling of the oxide scale can occur according to the first mechanism.

Which one of the two mechanisms proposed for partial spalling of the spinel layer applies in the case of P122 is not yet completely clear. The porosity in the oxide scale shown in Figure 13 (top) and remnants of oxide (spinel) on the surface of the Cr-depleted peak in the light-optical micrographs in Figure 14 imply that partial spalling is due to Fe-diffusion in the scale. On the other hand, the globular shape of the peak shown in the electron-optical micrograph in Figure 14 may have resulted from inward-diffusion of Fe before the scale spalled off. With respect to the oxidation behaviour of P122 subsequent to partial spalling, it would be less critical if only the outer part of the spinel layer spalls off (Fe-diffusion in the scale) and the inner, Cr-rich part remains on the top of the peak. If the whole scale spalls off from the top of the peak (Fe-diffusion in the steel), accelerated corrosion of the Cr-depleted steel is likely.

3.1.4 Quantitative influence of the oxygen content of the LBE

The most important result of the quantification of the metal recession after exposure under varying conditions with respect to the oxygen content of the LBE (which was performed according to the method described in Section 3.1.1, pp.14-15) is that, after ~5000 h, the material consumption is significantly lower than at permanently high oxygen content of the LBE ($c_O \approx 5\times10^{-7}$ mass-% ($a_{PbO} \approx 10^{-3}$); Figure 24). This lower material consumption results from the periods of low oxygen content of the LBE during which the driving force for oxygen transport (through the oxide scale) to the oxide scale/steel interface was also low. The establishment of oxides which are richer in Cr in comparison to the (Fe,Cr) spinel which forms at permanently high oxygen content of the LBE may have additionally reduced the oxygen transfer to this interface where the scale continued to grow. A significant reduction of the oxidation rate which per-

sists when the conditions change from low to high oxygen content was reached only locally in the case of P122, where, depending on the conditions for Cr-supply from the steel, an exceptionally Cr-rich oxide layer established during periods of low oxygen content of the LBE.

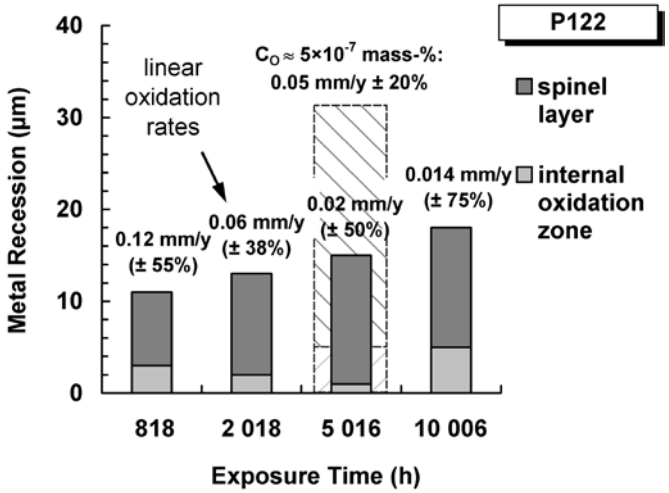

Figure 24 – *Metal recession (and resulting linear oxidation rates) of P122 after exposure to oxygen-containing flowing LBE at 550°C as estimated from the observed thicknesses of the spinel layer and the internal oxidation zone (mean values of twelve measurements each in a light-optical microscope at 500× magnification). Solid columns: the respective specimens were exposed to varying conditions with respect to the oxygen content (c_O between 5×10^{-10} and 5×10^{-6} mass-%). Hatched column: after exposure for 4990 h at $c_O \approx 5\times10^{-7}$ mass-%. The value for 5016 h was obtained from the reverse (non-aluminised) side of a GESA-treated specimen (ground instead of turned surface). In the case of the exposure for 10,006 h, only one domain of the surface (that shown in Figure 21) could be evaluated, since for all other sites along the specimen circumference in the examined vertical cross-section more or less pronounced spalling of the spinel layer was evident.*

3.1.5 P122 surface-alloyed with aluminium

Results of experiments on the oxidation behaviour of P122 surface-alloyed with aluminium are currently available after exposure at 550°C for 818, 2018 and 5016 h. During all these experiments, the oxygen content of the LBE varied and was mostly significantly lower than 10^{-6} mass-% (Table 4). An on-going experiment for 10,006 h at permanently high oxygen content around 5×10^{-7} mass-% will be finished in November 2005.

Figures 25 and 26 show light-optical micrographs of vertical cross-sections of the aluminised surface layer after the exposure experiments. Except for some oxidation along defects in the aluminised layer which were observed after the exposure for 5016 h (Figure 25 right), neither significant oxidation nor liquid metal corrosion occurred. Probably, a thin scale consisting of an Al- (and Cr-) rich mixed-oxide of type α-M_2O_3 formed on the surface and inhibited further oxidation of the aluminised layer. The Al and Cr content of the surface layer was about 12 and 9 mass-%, respectively (see section 2.2, pp. 4-5).

Figure 25 additionally shows that, in the course of the exposure for 5016 h, some changes in the microstructure occurred at the interface between the surface layer

and the bulk of the steel. Pores may have formed at this interface due to diffusion of Al into the bulk of the steel which is faster than diffusion of Fe, Cr etc. from the bulk into the surface layer. Another possibility is the precipitation of an intermetallic phase. During the exposures for 818 and 2018 h such obvious changes in the microstructure were not observed.

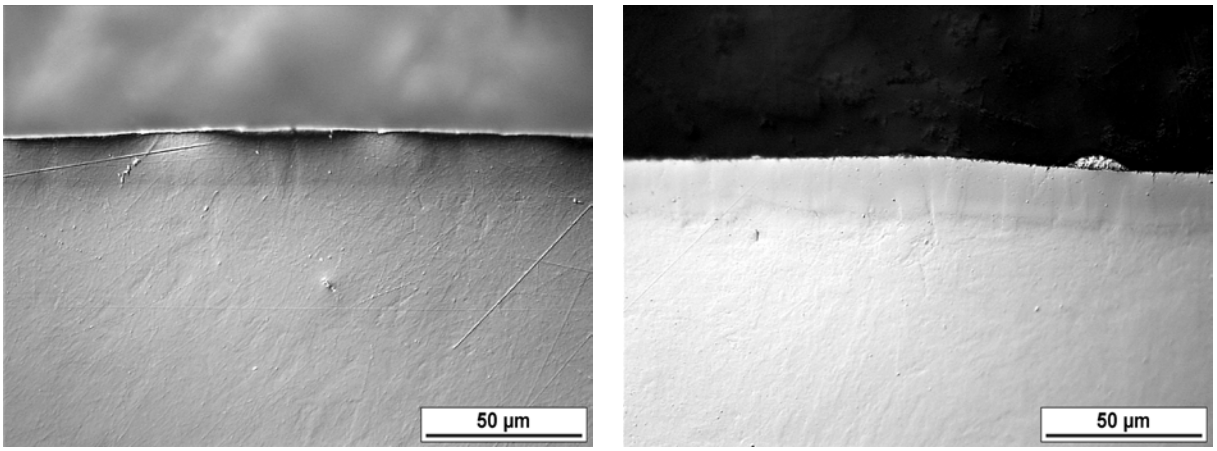

Figure 25 – *Vertical cross-section of the aluminised surface layer on GESA-treated P122 after exposure for 818 (left) and 2018 h (right) to flowing LBE at 550°C under varying conditions with respect to the oxygen content of the LBE (5×10^{-9} mass-% $\leq c_O \leq 5\times10^{-6}$ mass-%; $10^{-5} \leq a_{PbO} \leq 10^{-2}$). Light-optical micrographs using polarised illumination.*

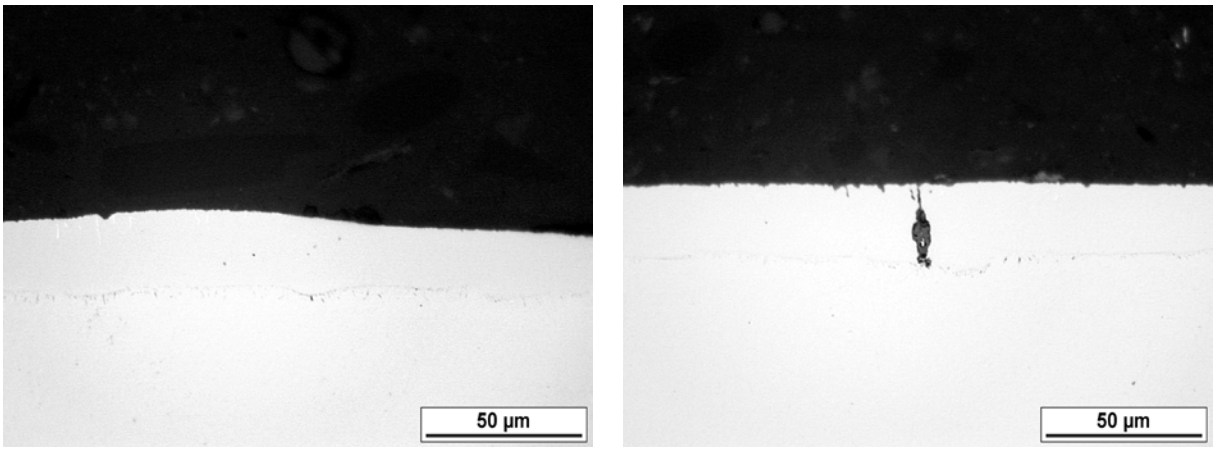

Figure 26 – *Light-optical micrographs of the aluminised surface layer on GESA-treated P122 after exposure for 5016 h to flowing LBE at 550°C. The oxgen content of the LBE varied between 5×10^{-10} and 5×10^{-6} mass-%. ($10^{-6} \leq a_{PbO} \leq 10^{-2}$).*

3.2 9Cr-2W ODS-steel

3.2.1 Oxidation behaviour at 550°C and $c_O \approx 5\times10^{-7}$ mass-% ($a_{PbO} \approx 10^{-3}$)

Cross-sections of the scale which covers the surface of ODS after the exposure to flowing LBE at 550°C and $c_O \approx 5\times10^{-7}$ mass-% ($a_{PbO} \approx 10^{-3}$) for 4990 h are shown in Figure 27. At the oxide scale/LBE interface, an (Fe,Cr) spinel layer with a mean thickness of 16 µm has formed. The inner part of the scale consists of a considerably

thicker internal oxidation zone (IOZ) in which Cr-rich oxides (Cr-rich spinel, Cr-rich α-M_2O_3 or chromia) precipitated mostly along grain boundaries within the exceptionally fine-grained steel. A XRD-spectrum recorded from the scale surface after removal of adherent LBE in hot fat confirms the formation of cubic Fe-Cr mixed-oxides like (Fe,Cr) spinel (Figure 28).

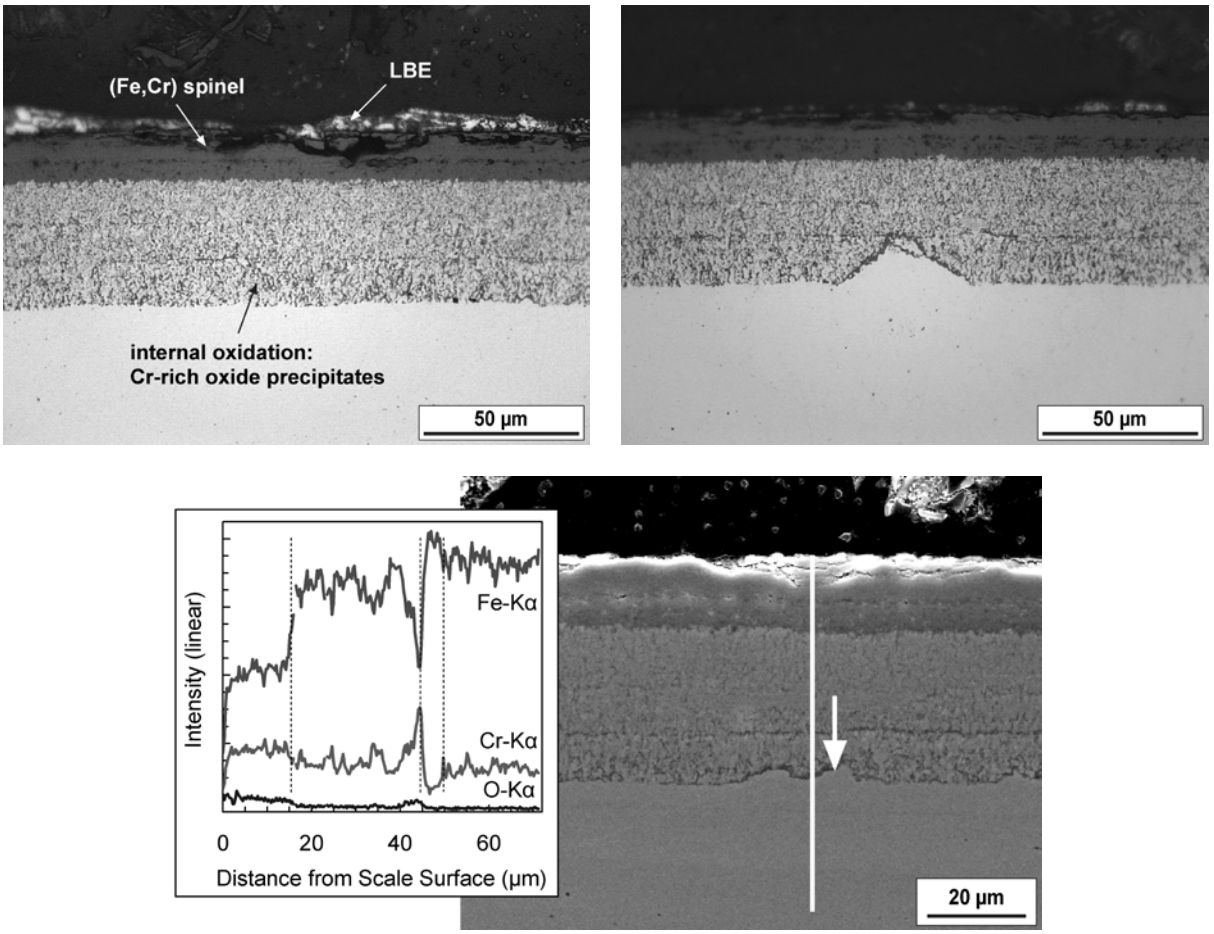

Figure 27 – *Oxide scale on the surface of the 9Cr-2W ODS-steel after exposure to flowing LBE at 550°C and $c_O \approx 5\times10^{-7}$ mass-% ($a_{PbO} \approx 10^{-3}$) for 4990 h. Top: light-optical micrographs of a vertical cross-section. Bottom: electron-optical micrograph of a longitudinal cross-section and qualitative EDX-linescan.*

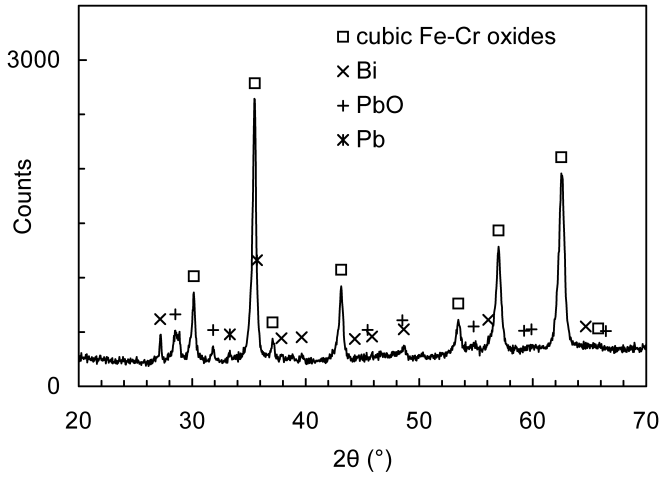

Figure 28 – *XRD-spectrum recorded from the surface of ODS after exposure to flowing LBE at 550°C and $c_O \approx 5\times10^{-7}$ mass-% ($a_{PbO} \approx 10^{-3}$) for 4990 h. Adherent LBE was removed by rinsing in hot fat. Cubic Fe-Cr oxides can be magnetite, Fe_3O_4, (Fe,Cr) spinel, $FeCr_2O_4$, or maghaemite, γ-Fe_2O_3. γ-Fe_2O_3 is only metastable under the exposure conditions.*

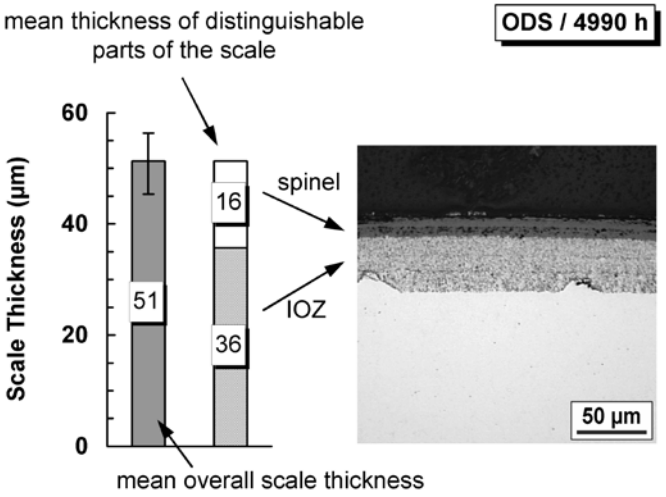

Figure 29 – *Mean thickness of the oxide scale on the surface of ODS after exposure to flowing LBE at 550°C and $c_O \approx 5\times10^{-7}$ mass-% ($a_{PbO} \approx 10^{-3}$) for 4990 h. The error bar indicates the deviation of the maximum and minimum, respectively, of 12 measurements from the mean value.*

A closer look at the IOZ reveals a layered sub-structure (Figure 27). Obviously, the precipitation of Cr-rich oxide occasionally resulted in a thin Cr-rich oxide layer which formation was probably favoured by the exceptionally fine-grained structure of the steel (fast Cr-diffusion along grain boundaries). A slight Cr-depletion of the steel (~2 µm) was observed beneath such a layer (Figure 27 bottom). However, a continuous Cr-rich layer with a long-lasting effect on the progress of internal oxidation did not form during the exposure for 4990 h, indicated by two or three of these layers in the cross-section. As implied by Figure 27, local peculiarities of the steel microstructure can promote the formation of a partially continuous Cr-rich oxide layer at the IOZ/steel interface, which reduces the local oxidation rate probably only temporarily.

Figure 29 summarises the results of measurements of the scale thickness on ODS after the exposure for 4990 h at $c_O \approx 5\times10^{-7}$ mass-% ($a_{PbO} \approx 10^{-3}$). 12 measurements were performed at sites uniformly distributed along the circumference of the specimen in the vertical cross-section investigated. With the assumption that the surface of the spinel layer coincides with the original position of the steel surface, a mean linear oxidation rate (in terms of metal recession) of 0.09 mm/y (± 12%) results from these measurements, with internal oxidation accounting for most of the metal recession. No Fe-oxide was found on the surface of the oxide scale for reasons which were discussed in section 3.1.1 (pp. 15-17). At least the Fe which was displaced by the inward-growth of the spinel dissolved in the LBE after diffusion towards the scale surface, i.e., a volume corresponding to approximately half the thickness of the spinel layer (p. 17). With a density of α-Fe of 7.86 g/cm³, the minimum amount of Fe dissolved in the LBE is ~0.06 g/cm² after 4990 h.

3.2.2 Behaviour under varying conditions with respect to the oxygen content

After the exposure for 818 h under varying conditions with respect to the oxygen content of the LBE (5×10^{-9} mass-% $\leq c_O \leq 5\times10^{-6}$ mass-% or $10^{-5} \leq a_{PbO} \leq 10^{-2}$), the scale

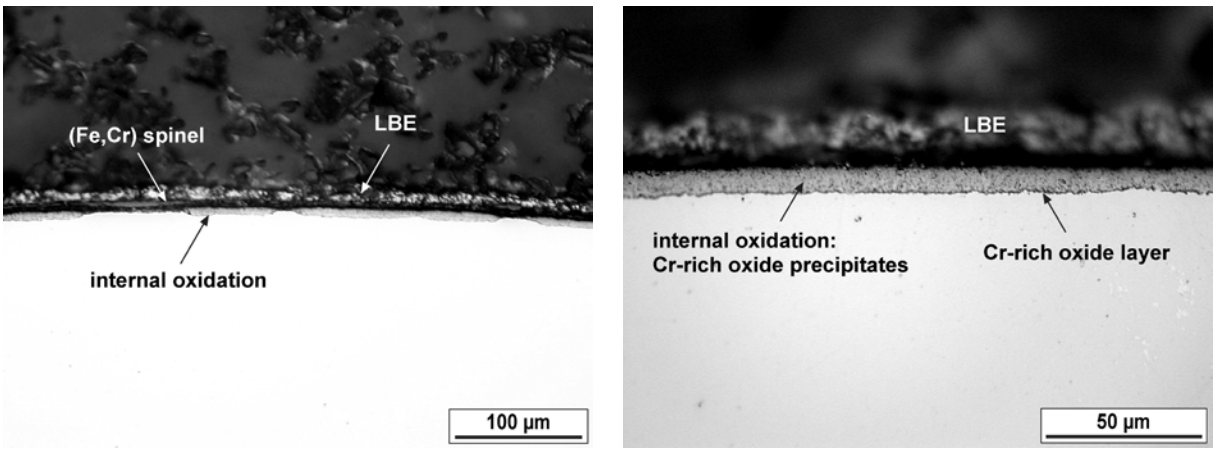

Figure 30 – *Oxide scale on the surface of ODS after exposure for 818 h to flowing LBE at 550°C. The oxygen concentration in the LBE varied between 5×10^{-9} and 5×10^{-6} mass-% ($10^{-5} \leq a_{PbO} \leq 10^{-2}$). Light-optical micrographs. In the right micrograph, the spinel layer is out of focus and appears as a diffuse gap between the LBE and the IOZ because of "edge-rounding" during the preparation.*

on the surface of ODS consists of an (Fe,Cr) spinel layer and an internal oxidation zone, from which the IOZ mostly is slightly thicker than the spinel layer (Figure 30). At the IOZ/steel interface, a thin layer of Cr-rich oxide has formed. After 2018 h, the IOZ has nearly completely disappeared and a compact oxide layer (with a multi-layered sub-structure) is observed where the IOZ was before (Figure 31). Except for those sites where Fe-oxide (magnetite, Fe_3O_4) formed on top of the spinel layer (Figure 31 right), the thickness of the oxide scale after 2018 h approximately coincides with the sum of the thickness of the spinel layer and the IOZ after 818 h, so that, in the main, only a transformation of the IOZ into an oxide layer took place during the 1200 h which lay between the two exposure times. A thin layer of Cr-rich oxide is still present at the oxide scale/steel interface, and Cr-depletion of the steel (a reduction of approximately 4 mass-% at the interface) occurred up to a depth of ~8 µm [8].

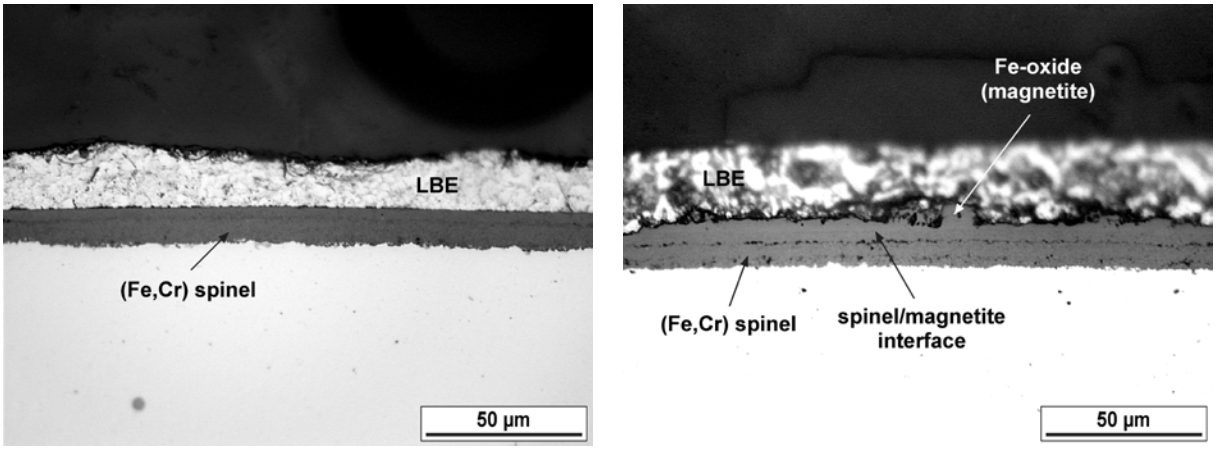

Figure 31 – *Oxide scale on the surface of ODS after exposure for 2018 h to flowing LBE at 550°C. The oxygen concentration in the LBE varied between 5×10^{-9} and 5×10^{-6} mass-% ($10^{-5} \leq a_{PbO} \leq 10^{-2}$). Left: domain with spinel layer. Right: local magnetite formation on top of the spinel layer.*

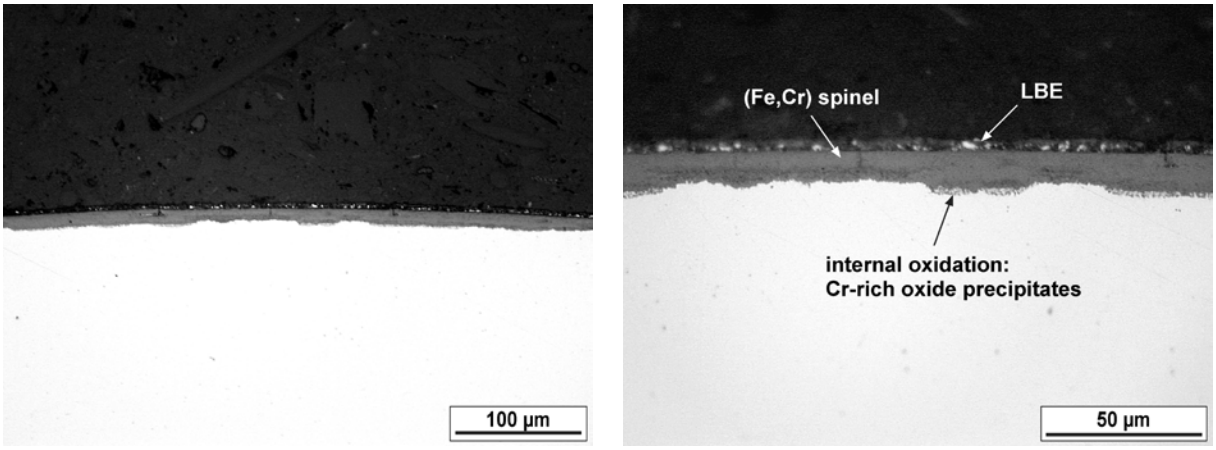

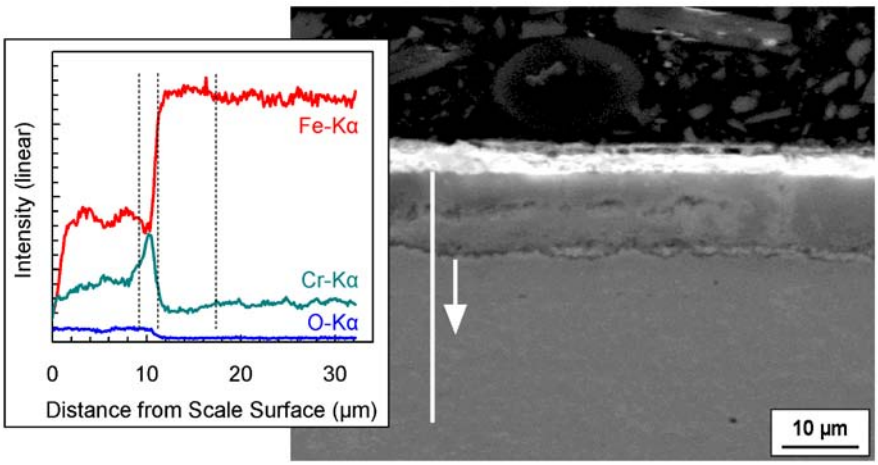

Figure 32 – *Oxide scale on the surface of ODS after exposure for 5016 h to flowing LBE at 550°C (non-aluminised part of GESA-treated specimen). The oxygen concentration in the LBE varied between 5×10^{-10} and 5×10^{-6} mass-% ($10^{-6} \leq a_{PbO} \leq 10^{-2}$). Top: light-optical micrographs of the scale. Bottom: electron-optical micrograph and qualitative EDX-linescan across the scale.*

The reverse side (non-aluminised part) of the GESA-treated specimen of ODS which was exposed for 5016 h under varying conditions with respect to the oxygen content (5×10^{-10} mass-% $\leq c_O \leq 5\times10^{-6}$ mass-% or $10^{-6} \leq a_{PbO} \leq 10^{-2}$) also shows a comparatively thin spinel layer and only slight local internal oxidation. Cr is enriched in the inner part of the oxide scale, in a narrow zone at the interface with the steel (Figure 32). Since, in the case of ODS, the steel surface was not specifically prepared for the GESA-treatment, the reverse side is representative for ODS surface-finished by turning, so that the observations can be directly compared with the results for ODS after exposure for 4990 h at permanently high oxygen content of the LBE. This comparison clearly shows that, at varying (mostly low) oxygen content of the LBE, ODS is much less susceptible to internal oxidation which accounts for the biggest part of the metal recession after the exposure at $c_O \approx 5\times10^{-7}$ mass-% ($a_{PbO} \approx 10^{-3}$) for approximately equal times (Figure 27). The lower susceptibility to internal oxidation results from the formation of a closed Cr-rich oxide layer (probably a slow-growing oxide of type α-M_2O_3) at the oxide scale steel interface which is promoted by the periods of low oxygen content of the LBE (during which Cr-diffusion from the bulk of the steel to this interface outweighed oxygen transfer through the spinel layer) in the course of the exposure under varying conditions (Figure 9). Additionally, the exceptionally fine-grained microstructure of ODS (fast Cr-diffusion along grain boundaries) and preferential nucleation at oxides dispersed in the steel (especially yttria) may have supported the formation of a closed Cr-rich oxide layer at the oxide scale/steel interface.

As long as the Cr-rich oxide layer at the oxide scale/steel interface persists, the further progress of the oxidation process is significantly hampered. Obviously, such a layer already formed during the period of low content at the end of the exposure for 818 h, so that the comparatively high oxygen content in the following 1200 h up to 2018 h (Figure 9) merely resulted in the transformation of the initially formed IOZ into spinel, with the displaced Fe having dissolved in the LBE (*cf.* p. 17); the Cr-depletion of the steel after the exposure for 2018 h indicates that Cr-transport from the bulk of the steel could maintain the protective properties of the Cr-rich layer during periods of high oxygen content of the LBE. This trend in the oxidation behaviour of ODS under varying conditions did also hold for the specimen which was exposed for 10,006 h, 5016 h under varying conditions and an additional 4990 h at permanently high oxygen content (Figure 33).

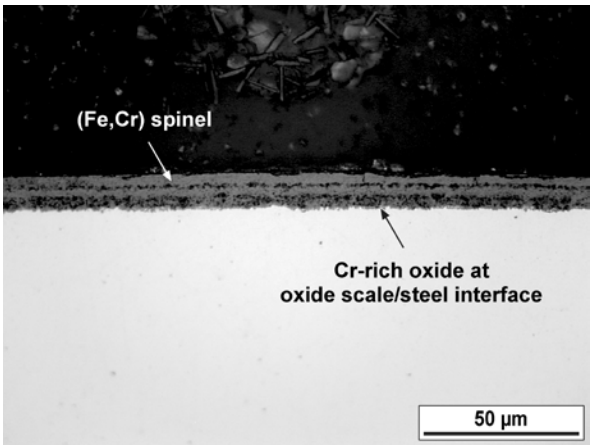

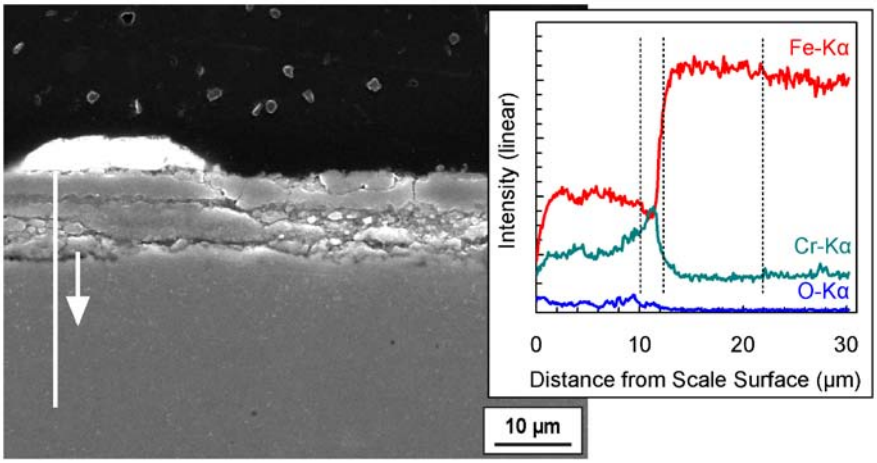

Figure 33 – *Oxide scale on the surface of ODS after exposure for 10,006 h to flowing LBE at 550°C (non-aluminised part of GESA-treated specimen). The oxygen concentration in the LBE varied between 5×10^{-10} and 5×10^{-6} mass-% ($10^{-6} \leq a_{PbO} \leq 10^{-2}$) and was ~$5\times10^{-7}$ mass-% ($a_{PbO} \approx 10^{-3}$) during the last 4990 h of the exposure experiment. Top: light-optical micrograph of the scale in vertical cross-section. Bottom: electron-optical micrograph of a longitudinal cross-section and qualitative EDX-linescan across the scale.*

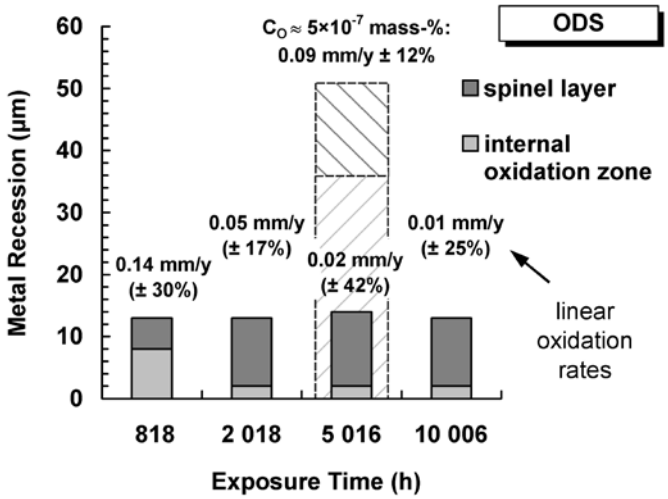

Figure 34 – *Metal recession (and resulting linear oxidation rates) of ODS after exposure to oxygen-containing flowing LBE at 550°C as estimated from the observed thicknesses of the spinel layer and the internal oxidation zone (mean values of twelve measurements each in a light-optical microscope at 500× magnification). Solid columns: the respective specimens were exposed to varying conditions with respect to the oxygen content (c_O between 5×10^{-10} and 5×10^{-6} mass-%). Hatched column: after exposure for 4990 h at $c_O \approx 5\times10^{-7}$ mass-%.*

The measurements of the scale thickness after the exposure under varying conditions with respect to the oxygen content of the LBE and the resulting metal recessions (estimated as introduced in Section 3.1.1, pp. 14-15) confirm the observations of the other post-test examinations (Figure 34). The reduction in linear oxidation rate due to periods of low oxygen content of the LBE is in the range of one order of magnitude. No liquid metal corrosion occurred, even if the oxygen content temporarily was as low as 5×10^{-10} mass-% ($a_{PbO} = 10^{-6}$). But it should be emphasized that all experiments started with high oxygen content of the LBE.

3.2.3 ODS surface-alloyed with aluminium

Results of experiments on the oxidation behaviour of ODS surface-alloyed with aluminium are currently available after exposure at 550°C for 818, 2018 and 5016 h. During all these experiments, the oxygen content of the LBE varied and was mostly significantly lower than 10^{-6} mass-% (Table 4). An on-going experiment for 10,006 h at permanently high oxygen content around 5×10^{-7} mass-% will be finished in November 2005.

Figure 35 is representative for the aluminised surface layer on GESA-treated ODS after the exposure for 818 h. Neither liquid metal corrosion nor significant oxidation occurred, indicating that a thin oxide scale, which probably consists of an Al- (and Cr-) rich mixed-oxide of type α-M_2O_3, protects the surface of the aluminised layer. The same behaviour was observed after the exposure for 2018 h (Figure 36), with only few exceptions, in case of which a less protective oxide (probably of spinel type) locally formed (Figure 36 right). A local peculiarity of the composition of the aluminised layer may be responsible for the formation of the less protective oxide [8]. After the exposure for 5016 h, neither liquid metal corrosion nor significant oxidation was observed (Figure 37). The Al- and Cr-content of the surface layer was about 6 and 8 mass-%, respectively (see Section 2.2, pp. 4-5).

A change in the microstructure at the interface between the surface layer and the bulk of the steel, as was observed after the exposure of GESA-treated P122 for 5016 h (see Section 3.1.5, p. 26), did not occur in the case of GESA-treated ODS. Possible reasons for this finding might be fast diffusion of Cr and Fe in the exceptionally fine-grained microstructure of ODS and a different composition of the surface layer on P122 and ODS.

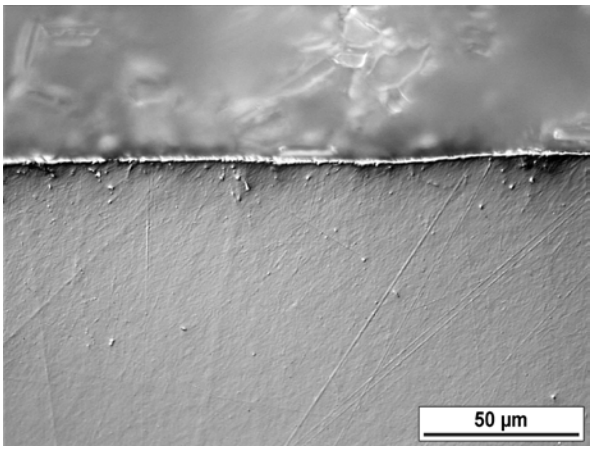

Figure 35 – *Vertical cross-section of the aluminised surface layer on GESA-treated ODS after exposure for 818 h) to flowing LBE at 550°C under varying conditions with respect to the oxygen content of the LBE (5×10^{-9} mass-% $\leq c_O \leq 5\times10^{-6}$ mass-%; $10^{-5} \leq a_{PbO} \leq 10^{-2}$). Light-optical micrograph using polarised illumination.*

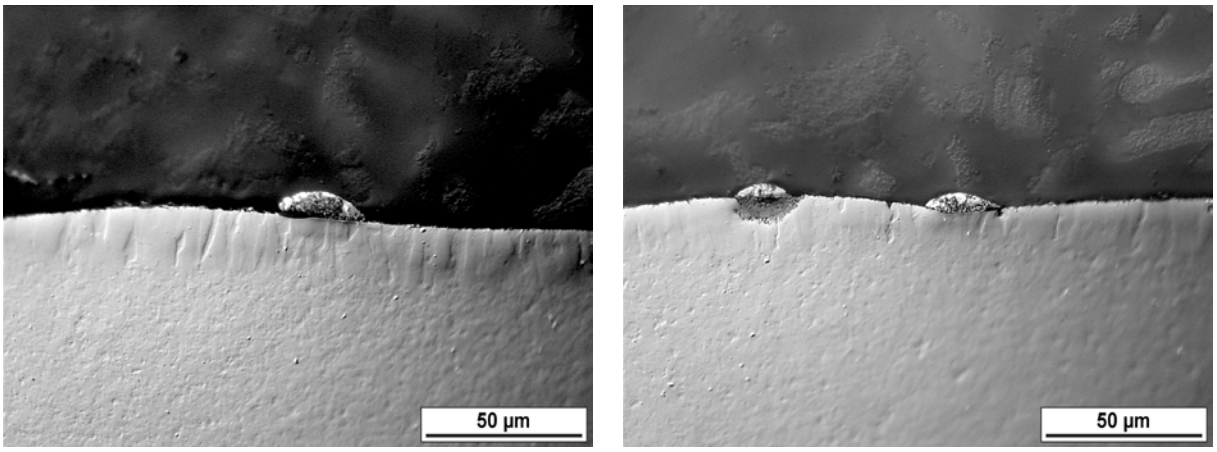

Figure 36 – *Vertical cross-section of the aluminised surface layer on GESA-treated P122 after exposure for 2018 h to flowing LBE at 550°C under varying conditions with respect to the oxygen content of the LBE (5×10^{-9} mass-% $\leq c_O \leq 5\times10^{-6}$ mass-%; $10^{-5} \leq a_{PbO} \leq 10^{-2}$). Light-optical micrographs using polarised illumination.*

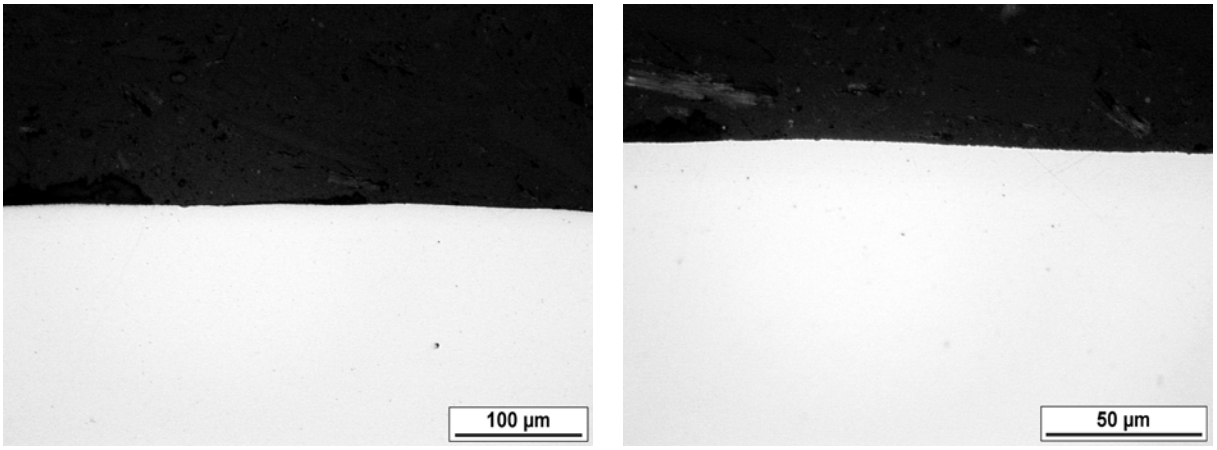

Figure 37 – *Light-optical micrographs of the aluminised surface layer on GESA-treated P122 after exposure for 5016 h to flowing LBE at 550°C. The oxgen content of the LBE varied between 5×10^{-10} and 5×10^{-6} mass-%. ($10^{-6} \leq a_{PbO} \leq 10^{-2}$).*

4 Comparison with Results for Stagnant LBE

In another part of this study on oxidation in LBE, P122 and ODS (with and without GESA-treatment) were exposed to stagnant LBE at temperatures between 500° and 650°C in the COSTA device at the Institute for Pulsed Power and Microwave Technology. In these experiments, the main part of cuboidic specimens (27×6×2 mm) was immersed in a ceramic crucible which contained the molten LBE, and the whole arrangement was flushed with an oxygen-containing gas. The gas composition was chosen so that, for thermodynamic equilibrium between the LBE and the gas, oxygen contents of 10^{-4}, 10^{-6} and 10^{-8} mass-%, respectively, resulted in the LBE during the various experiments. The findings of these experiments have already been reported

[5,21-23]. Results on exposure experiments in stagnant LBE at 550°C and $c_O = 10^{-6}$ mass-%, which are comparable with respect to temperature and oxygen content with the exposures at constantly high oxygen content in the CORRIDA loop, can be found in References 5 and 22. Examples of the oxide scales which formed on the surface of P122 and ODS are shown in Figure 38 and 39.

The principal parts of the oxide scales which formed in the course of the exposure in the CORRIDA loop at $c_O \approx 5\times10^{-7}$ mass-% ($a_{PbO} \approx 10^{-3}$) – the spinel layer and an internal oxidation zone (diffusion zone) – were also observed in the case of the COSTA experiments at $c_O = 10^{-6}$ mass-%. However, Fe-oxide (magnetite) did more frequently form on top of the spinel layer, especially in the case of ODS. When considering that the Fe-oxide formation competes with Fe dissolution in the LBE, this finding implies that the comparatively small, stagnant mass of LBE in the crucible is saturated with Fe, at least immediately at the specimen (oxide scale) surface. In the test-sections of the CORRIDA loop (T = 550°C), Fe saturation is much less likely to occur, because the ratio of the mass of the specimens to the mass of circulating LBE is much lower and, additionally, dissolved Fe is transported by the flow towards sections of the loop with significantly lower temperature (550°C ≤ T ≤ 380°C), where Fe partially re-

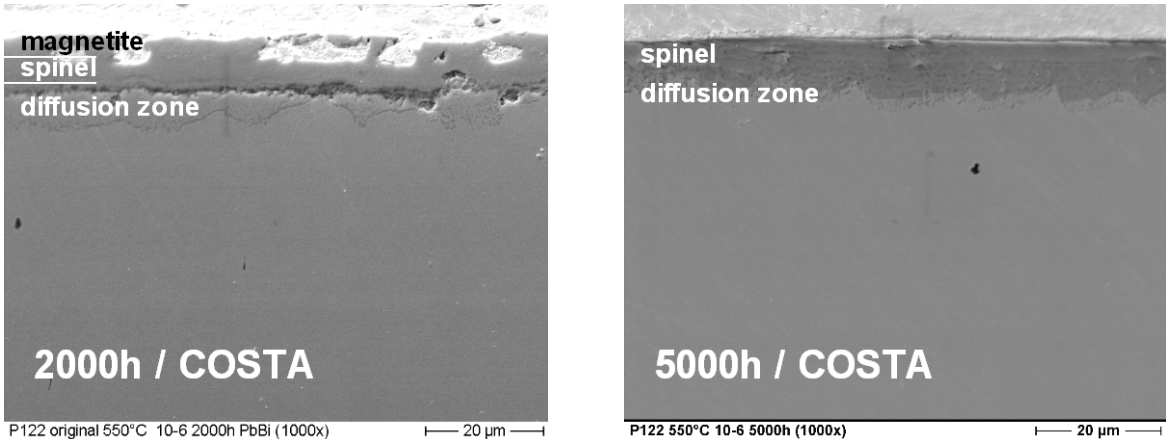

Figure 38 – *Vertical cross-section of P122 after exposure at 550°C and $c_O = 10^{-6}$ mass-% in the COSTA device. Left: after 2000 h. Right: after 5000 h. Note that the internal oxidation zone is denoted as diffusion zone, emphasising that oxygen diffusion into the steel is involved in the formation of oxide precipitates in the steel.*

precipitates (most likely in the form of oxide). Whether saturation with Fe and formation of Fe-oxide occurs at an oxidised specimen surface, depends on the Fe activity at the surface of the oxide scale, i.e., the Fe-content of the spinel, and also on the oxygen content (activity) of the LBE. When comparing P122 and ODS, the Fe-content of the spinel layer should be slightly higher in the case of ODS, which can explain the higher tendency to form Fe-oxide in the presence of oxygen-containing LBE. The exceptional occurrence of Fe-oxide on top of the spinel layer on ODS in the course the exposure for 2018 h in the CORRIDA loop (Figure 31 right) is probably due to the temporarily high oxygen content during this exposure period (Figure 9). Since Fe-oxide was only locally present in this case, local peculiarities of the spinel composition and/or mass-transport in the LBE may have promoted Fe-oxide formation. (See also Section 3.1.1, pp. 15-17).

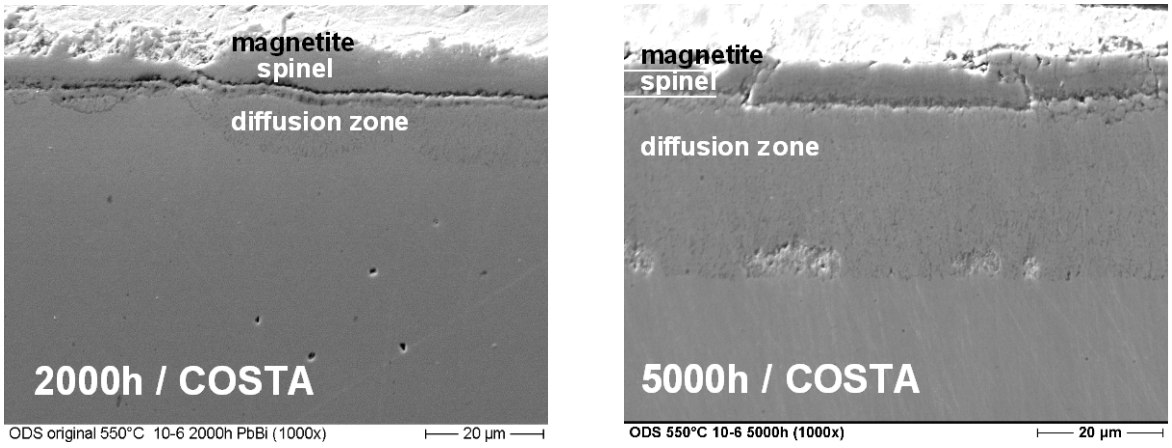

Figure 39 – *Vertical cross-section of ODS after exposure at 550°C and $c_O = 10^{-6}$ mass-% in the COSTA device. Left: after 2000 h. Right: after 5000 h. Note that the internal oxidation zone is denoted as diffusion zone, emphasising that oxygen diffusion into the steel is involved in the formation of oxide precipitates in the steel.*

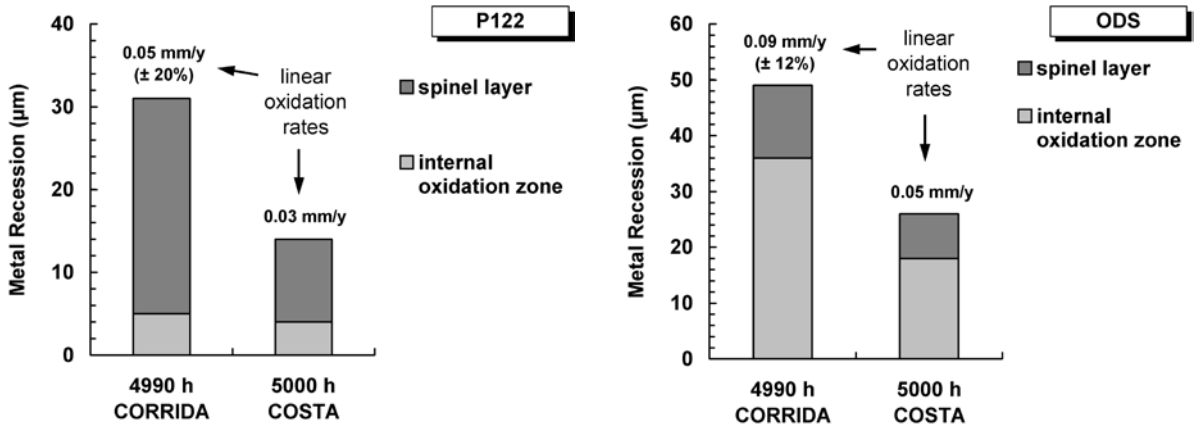

Figure 40 – *Comparison of the CORRIDA and COSTA experiments with respect to the metal recession of P122 (left) and ODS (right) after exposures at 550°C for ~5000 h. The oxygen content was $c_O \approx 5\times10^{-7}$ mass-% ($a_{PbO} \approx 10^{-3}$) and $c_O = 10^{-6}$ mass-%, respectively. The metal recession was estimated using the thickness of the spinel layer and the internal oxidation zone.*

A quantitative comparison of the CORRIDA and COSTA experiments after exposure times round about 5000 h is shown in Figure 40. The metal recession which follows from the thickness of the spinel layer and the internal oxidation zone (diffusion zone) is higher in the case of the CORRIDA experiments for both P122 and ODS. The observed difference may at least partly be due to the specific conditions for the dissolution of Fe in the LBE, which apparently is an essential sub-process of the oxide scale formation. Additionally, oxygen is more efficiently transported to the specimen surface under flowing conditions (convective transport) than in stagnant LBE (only oxygen diffusion).

As well as the exposures in the CORRIDA loop, the COSTA experiments showed that surface-alloying with aluminium significantly reduces the oxidation of both steels investigated.

5 Conclusions

Both P122 and ODS showed a promising oxidation behaviour in flowing LBE at 550°C and $c_O \approx 5\times10^{-7}$ mass-% ($a_{PbO} \approx 10^{-3}$). The spinel layer which forms under such conditions prevents liquid-metal corrosion of the steels, with the mean oxidation rate being less than 0.1 mm/y during 4990 h of exposure. In the case of ODS, internal oxidation accounts for the biggest part of the metal recession which amounts about 0.09 mm/y (±12%). P122 exhibits a lower mean oxidation rate in the range of 0.05 mm/y (±20%). Since the Cr-content of P122 is close to the (theoretical) minimum for the formation of a continuous chromia scale, the local oxidation rates can significantly differ from each other, i.e., where a thin layer of Cr-rich α-M_2O_3 protects the surface of P122, the local oxidation rate is much lower than in domains where this protective scale broke down and spinel formation (accompanied by internal oxidation) set in. The different local oxidation rates result in a considerable non-uniformity of the instantaneous steel surface which consequently influences the adhesion of the oxide scale. Around pronounced non-uniformities (peaks) in the surface-profile, the scale on P122 is prone to partial spalling. The subsequent behaviour of the steel depends on the mechanisms of scale spalling, two of which have been discussed in Section 3.1.3. The peculiar behaviour of P122 particularly depends on the surface-finish of the steel and is the more pronounced the higher the deformation of the near-surface part of the steel.

Experiments, during which the oxygen content significantly varied, showed that periods of low oxygen content can significantly reduce the oxidation rate of the steels. This reduction in the metal recession is especially pronounced for ODS due to the formation of a Cr-rich oxide layer at the oxide scale/steel interface which prevents the progress of internal oxidation of this exceptionally fine-grained steel. As long as this Cr-rich layer is maintained by sufficient supply of Cr from the bulk of the steel, further oxidation is negligible. The protective property of the Cr-rich oxide layer at least temporarily (~5000 h) persists also if the oxygen content is raised again, so that periods with low oxygen content of the LBE can significantly prolong the life-time of thin-walled components made of ODS in plants using liquid-heavy-metal technology. Since P122 exhibits a comparatively low oxidation rate at high oxygen content of the LBE, the reduction during periods of low oxygen content is less pronounced in the case of this steel. A Cr-rich inner part of the scale, the protective properties of which persists during periods of high oxygen content of the LBE, apparently forms only locally.

In the case of both steels, the spinel layer which forms during periods of high oxygen content of the LBE prevents liquid-metal corrosion even if the oxygen content temporarily is as low as 5×10^{-10} mass-% ($a_{PbO} = 10^{-6}$).

Surface-alloying with aluminium protects the steels from remarkable oxidation and liquid metal-corrosion. Such protective surface layers can be produced by the GESA-treatment. However, some improvements of this treatment are necessary to prevent defects in the aluminised layer.

The mean oxidation rates observed after exposure to flowing LBE (CORRIDA-experiments) are slightly higher than oxidation rates following from experiments with stagnant LBE (COSTA-experiments). This difference may at least partly be due to the specific conditions for the dissolution of Fe in the LBE, which apparently is an essential sub-process of the oxide scale formation. Additionally, oxygen is more efficiently transported to the specimen surface under flowing conditions than in stagnant LBE.

References

[1] *Phase Diagrams of Binary Iron Alloys*, ed. H. Okamoto (Materials Park, OH: ASM International, 1993).

[2] P.J. Ennis, A. Zielińska-Lipiec, A. Czyrska-Filemonowicz, Mater. Sci. Technol. 16 (2000) 1226-1232.

[3] P.J. Ennis, A. Czyrska-Filemonowicz, Sādhanā 28 (2003) 709-730.

[4] V. Engelko, B. Yatsenko, G. Müller, H. Bluhm, Vacuum 62 (2001) 211-216.

[5] G. Müller, G. Schumacher, A. Weisenburger, A. Heinzel, F. Zimmermann, T. Furukawa, K. Aoto, *Study on Pb-Bi Corrosion of Structural and Fuel Cladding Materials for Nuclear Applications – Part I: Corrosion investigation of steels after 800 and 2,000h exposure to stagnant liquid Pb-Bi at elevated temperatures*, JNC TY9400 2002-016 (Japan Nuclear Cycle Development Institute, 2002).

[6] J. Konys, H. Muscher, Z. Voß, O. Wedemeyer, J. Nucl. Mater. 296 (2001) 289-294.

[7] H. Muscher, J. Konys, Z. Voß, O. Wedemeyer, *Measurement of Oxygen Activities in Eutectic Lead-Bismuth by Means of the EMF Method*, Report FZKA 6690 (Forschungszentrum Karlsruhe GmbH, Germany, 2001).

[8] C. Schroer, Z. Voß, O. Wedemeyer, J. Novotny, J. Konys, A. Heinzel, A. Weisenburger, G. Müller, T. Furukawa, K. Aoto, *Study on Pb-Bi Corrosion of Structural and Fuel Cladding Materials for Nuclear Applications – Part V: Results of exposure experiments in oxygen containing flowing LBE at 550°C for 800 and 2000 h*, JNC TY9400 2004-032 (Japan Nuclear Cycle Development Institute, 2004).

[9] N.A. Gokcen, J. Phase Equilibria 13 (1992) 21-32.

[10] H.U. Borgstedt, C.K. Mathews, *Applied Chemistry of the Alkali Metals* (New York, London: Plenum Press, 1987) pp. 78-80.

[11] HSC Chemistry 5.0 (Pori, FIN: Outokumpu Research Oy, 2002).

[12] I.V. Kazakova, B.M. Lepinskikh, S.A. Lyamkin, *Effect of Alloying Elements on the Solubility of Oxygen in Pb-Bi melts*, Report UDK 669.4'76-154:541.8 (former Sverdlovsk, USSR: Academy of Science, Ural Department,1983), *in Russian*.

[13] Orlov et al. (1997), cited by G. Benamati, P: Buttol, C. Fazio, V. Imbeni, C. Martini, G. Palombarini, A. Rusanov, in: *Corrosion and Oxygen Control, Minutes of the Workshop on Heavy Liquid Metal Technology, September 16-17, 1999, Forschungszentrum Karlsruhe, Germany*, ed. J. Konys, Report FZKA 6389 (Forschungszentrum Karlsruhe GmbH, Germany, 1999) pp. 93-121.

[14] G. Müller, A. Heinzel, G. Schumacher, A. Weisenburger, J. Nucl. Mater. 321 (2003) 256-262.

[15] G. Müller, G. Schumacher, F. Zimmermann, J. Nucl. Mater. 278 (2000) 85-95.

[16] N. Birks, G.H. Meier, *Introduction to High Temperature Oxidation of Metals* (London: Edward Arnold (Publishers) Ltd., 1983) pp. 118-119.

[17] N. Birks, G.H. Meier, *ibid.* pp. 110-112.

[18] C. Piehl, Zs. Tökei, H.J. Grabke, Materials at High Temperatures 17 (2000) 243-246.
[19] C. Wagner, J. Electrochem. Soc. 103 (1956) 571-580.
[20] Zs. Tökei, H. Viefhaus, H.J. Grabke, Applied Surface Science 165 (2000) 23-33.
[21] G. Müller, G. Schumacher, A. Weisenburger, A. Heinzel, F. Zimmermann, T. Furukawa, K. Aoto, *Study on Pb-Bi Corrosion of Structural and Fuel Cladding Materials for Nuclear Applications – Part II: Corrosion investigation in stagnant Pb-Bi at 500, 550, 600 and 650°C after 5000 h of exposure,* JNC TY9400 2002-023 (Japan Nuclear Cycle Development Institute, 2002).
[22] G. Müller, G. Schumacher, A. Weisenburger, A. Heinzel, F. Zimmermann, T. Furukawa, K. Aoto, *Study on Pb-Bi Corrosion of Structural and Fuel Cladding Materials for Nuclear Applications – Part III: Corrosion investigation of steels between 500-650°C during 10,000 h of exposure to stagnant liquid Pb-Bi containing 10^{-6}wt% oxygen,* JNC TY9400 2003-026 (Japan Nuclear Cycle Development Institute, 2003).
[23] G. Müller, G. Schumacher, A. Weisenburger, A. Heinzel, F. Zimmermann, T. Furukawa, K. Aoto, *Study on Pb-Bi Corrosion of Structural and Fuel Cladding Materials for Nuclear Applications – Part IV: Corrosion investigation of steels between 500-650°C after 800, 2000 and 5000 h of exposure to stagnant liquid Pb-Bi containing 10^{-4} wt% and 10^{-8} wt% oxygen*, JNC TY9400 2003-028 (Japan Nuclear Cycle Development Institute, 2003).